THESIS FOR THE DEGREE OF DOCTOR OF PHILOSOPHY

Partial methane oxidation: insights from first principles and micro-kinetics calculations

ADAM A. ARVIDSSON

CHALMERS

Cover:
Illustration of an oxygen atom being surgically inserted into a C-H bond in a methane
molecule.

Partial methane oxidation: insights from first principles and micro-kinetics calculations
ADAM A. ARVIDSSON
Department of Physics
Chalmers University of Technology

Abstract

Partial methane oxidation is a much-desired reaction with some intriguing challenges. Not only is there a need to activate methane and oxygen, but there is also a need to control the selectivity and prevent over-oxidation to thermodynamically more stable products, like carbon dioxide and water. In fact, this is so difficult that at many oil extraction sites, methane, which inevitably accompanies the welled crude oil, is today flared since gas-phase methane is too inconvenient to store and transport.

In nature, there are enzymes that can partially oxidize methane to methanol at ambient pressure and temperature, although at a very slow rate. An often studied class of material with the potential of being an inorganic analogue to these enzymes are zeolites. Zeolites are a porous class of material that can readily be synthesized and that have been shown to convert methane to methanol at ambient conditions with a high selectivity, but with a low conversion. Unravelling the bottlenecks of this, as of yet, inefficient reaction, calls for an atomistic understanding of what is in fact controlling activity and selectivity of the catalysts at hand.

In this thesis, zeolites and chemically related structures, zeotypes, are studied using first-principles calculations combined with micro-kinetic modelling. As a first step, a candidate for the active site in these materials, the $[\text{Cu-O-Cu}]^{2+}$ motif, which is found primarily in the ZSM-5 zeolite, and its relevance for Cu, Ni, Co, Fe, Ag, and Au is investigated. Using a straightforward first-principles based micro-kinetic model, we find that this motif is only relevant for copper. Vibrational IR-spectra and temperature programmed desorption spectra are also calculated for monomer and dimer copper motifs in the ZSM-5 and SSZ-13 zeolites, and the results support experimental conclusions. When studying the continued reaction of methanol to dimethyl ether, large-scale trends in activity correlated to the acidity of the acid sites in three zeolite framework types have been determined, indicating that tuning acidity will change the selectivity between methanol and dimethyl ether.

The partial oxidation of methane is also studied using molybdenum sulfide clusters, Mo_6S_8. These small clusters enables studies of a wider reaction network, similar to the one in zeolites, where the oxygenated species are replaced by their sulfur-contaning counterparts. In this way, it allows investigation of the activity and selectivity towards methanethiol and dimethyl sulfide using different reaction mechanisms and different promoters. The reaction of methane with H_2S is used when cleaning sour natural gas, which is why, in this case, H_2S is used as the oxidant instead of oxygen. Our results show that the presence of some promoters on the sulfide clusters affect activity, while others affect selectivity. Furthermore, the results show that diffusion is important to include in the kinetic model.

Keywords: partial methane oxidation, density functional theory, microkinetic modelling, zeolites, zeolite acidity, molybdenum sulfide cluster

"The greatest teacher, failure is"

– Yoda

List of Publications

This thesis is based on the following appended papers:

I. Metal dimer sites in ZSM-5 zeolite for methane-to-methanol conversion from first-principles kinetic modelling: is the $[Cu\text{-}O\text{-}Cu]^{2+}$ motif relevant for Ni, Co, Fe, Ag, and Au?
Adam A. Arvidsson, Vladimir P. Zhdanov, Per-Anders Carlsson, Henrik Grönbeck, and Anders Hellman
Catal. Sci. Technol., **7** (2017), 1470-1477

II. Methanol Desorption from Cu-ZSM-5 Studied by *In Situ* Infrared Spectroscopy and First-Principles Calculations
Xueting Wang, Adam A. Arvidsson, Natalia M. Martin, Johan Nilsson, Stefan Carlson, Johan Gustafson, Magnus Skoglundh, Anders Hellman, and Per-Anders Carlsson
J. Phys. Chem. C 2017, 121, 27389-27398

III. Desorption Products during Linear Heating of Copper Zeolites with Preadsorbed Methanol
Xueting Wang, Adam A. Arvidsson, Magnus Skoglundh, Anders Hellman, and Per-Anders Carlsson
In manuscript

IV. The methanol-to-DME reaction in zeotypes: a first-principles based micro-kinetic study
Adam A. Arvidsson, Philipp N. Plessow, Anders Hellman, and Felix Studt
In manuscript

V. CH_4 and H_2S reforming to CH_3SH and H_2 catalyzed by metal promoted Mo_6S_8 cluster: a first-principles micro-kinetic study
William Taifan, Adam A. Arvidsson, Eric Nelson, Anders Hellman, and Jonas Baltrusaitis
Catal. Sci. Technol., 2017, **7**, 3546

VI. First-princples micro-kinetic study of CH_4 and H_2S catalytic conversion to methanethiol/dimethyl sulfide on Mo_6S_8 clusters: activity/selectivity of different promoters
Adam A. Arvidsson, William Taifan, Anders Hellman, and Jonas Baltrusaitis
Submitted to Catalysis Science & Technology

My contributions to the publications

Paper I
I performed all the calculations and wrote the first draft of the paper.

Paper II
I performed all the calculations and wrote the theoretical part of the paper.

Paper III
I performed all the calculations and wrote the theoretical part of the manuscript.

Paper IV
I performed all the calculations and wrote the first draft of the manuscript.

Paper V
I performed all microkinetic simulations and wrote the main part of the paper.

Paper VI
I formulated the reaction mechanism and performed all microkinetic simulations and co-authored the manuscript.

Contents

Chapter 1

Introduction

"
   Jag skall derföre, för att begagna en i kemien välkänd härledning, kalla den kroppars *katalytiska kraft*, sönderdelning genom denna kraft *katalys*, likasom vi med ordet analys beteckna åtskiljandet af kroppars beståndsdelar medelst den vanliga kemiska frändeskapen."[1]

– Jöns Jacob Berzelius [1]

Since ancient times catalysis has been used to speed up or steer chemical reactions, the most notable example being the fermentation of sugar to alcohol, where yeast is needed for the process to take place [2]. The first recorded mentioning of the word *catalysis* was by the German alchemist Andreas Libavius in 1597 [2, 3]. Although, his idea of catalysis would not correspond to our modern interpretation. The first person to describe the principal features of what we now know as catalysis, without naming it as such, was Elizabeth Fulhame in 1794 [2, 4]. She suggested that the presence of small quantities of water was necessary in order to oxidize carbon monoxide, but that the water remained unaffected after the reaction. Quite a few years later, in 1835, Jöns Jacob Berzelius introduced the term *catalysis*, deriving from the greek words *kata* meaning down, and *lyein* meaning loosen [5]. Berzelius ambition was, however, not to explain the new phenomenon, but rather to offer a classification, in the Linneaus tradition of naming and sorting things [6, 7]. Without mentioning the work by Fulhame, Berzelius gave a summary of experiments performed by others in the previous years, in the not so humbly called "Annual report on progress in physics and chemistry" [1]. Inspired by experiments carried out by Edmund and Humphry Davy in England, and Döbereiner and Mitscherlich in Germany, Berzelius realized that they all had observed the same, and so far unnamed, phenomenon. While trying to develop a safer lamp for coal miners, Humphry Davy recognized that a platinum wire, when exposed to oxygen and coal gas (methane), would glow white hot and was able to keep the wire of the lamp glowing even without a flame. Davy did not understand the phenomenon and described it as "more like magic than anything I have seen" [5, 8, 9]. Shortly after, Edmund Davy carried out experiments with platinum powder and observed that it reacted strongly with alcohol vapour at room temperature, remaining hot until all alcohol was consumed. Inspired by Davys' work, Johann Wolfgang Döbereiner noted that platinum also had extraordinary effects on hydrogen oxidation. With pure oxygen, the reaction was so violent that it charred the filter paper holding the platinum powder. However, it was Eilhard Mitscherlich's research on the formation of ether from

---

[1]Translation: "I shall, therefore, to use a well-known derivation in chemistry, call it bodies' catalytic force and the decomposition by this force catalysis, just as we signify by the word analysis the separation of the constituents of bodies by the usual chemical affinities."

alcohol when mixed with sulfuric acid that made Berzelius realize that it was the same phenomenon that Davy and Döbereiner had observed with platinum [1]. Berzelius realized that several materials, in solid form or in solution, could exert this enhancing influence, which could not be described by standard chemistry at that time. Since these substances seemed to partake in the chemical reactions, without being consumed themselves, Berzelius coined the new concept, *catalysis*. Following Berzelius, the field of catalysis expanded with the discovery of more and more catalytic reactions. The modern perception of catalysis in industrial processes is clearly formulated by Wilhelm Ostwald who supposedly said "there is no chemical reaction which can not be influenced catalytically" [2]. An important and often mentioned example of a catalytic reaction is the Haber-Bosch process in the beginning of the 20th century, which synthesises ammonia from hydrogen and nitrogen using an iron catalyst [10, 11]. This new process revolutionized global agriculture, since it made it possible to artificially produce fertilizer, allowing for a population growth from around 1 billion people in 1900 to around 7 billion today. Our understanding of the field of catalysis has since increased tremendously, and with the use of surface science and computational chemistry/physics the aim is to understand catalysis and catalysts all the way down to the atomistic scale.

Amongst the many catalytic reactions that are of high scientific and industrial interest, this thesis focuses on the partial oxidation of methane into, for instance, methanol. Such a reaction truly pushes the limits of our understanding of catalysis and our engineering skills, since it needs to both be efficient and selective, to avoid the over-oxidation of methane into carbon dioxide. The remainder of this introductory chapter will give a brief background for this thesis by motivating the work presented herein, give a brief background on catalysis as it developed in the centuries after Berzelius, briefly introduce zeolites, which are the main type of catalyst material for this reaction, and define the scope of the thesis.

1.1 Motivation

Why is partial methane oxidation interesting? The short answer is because so much methane is today wasted. The main reason is that methane is a gas, which is difficult to transport and store. If we were able to turn it into a liquid like methanol (partially oxidize methane), it would make us waste much less of this very useful energy source.

Methane is the main component of biogas and natural gas, along with smaller amounts of higher alkanes, such as ethane, propane and buthane [12]. The known reserves of natural gas were more than 190 trillion cubic meters at the end of 2017, which are enough to be able to sustain the global consumption of natural gas for more than half a century [13]. Unfortunately, much of these reserves are located in isolated areas, like offshore oil wells, where it is difficult to capture and store gases. Since methane has about 30 times the global warming potential (GWP) of carbon dioxide [14, 15], methane is flared (burned) into carbon dioxide and water. It is estimated that 3.5 %, or about 143 billion cubic metres, of the natural gas globally extracted was flared in 2012 [16]. Thanks to the low carbon emission per energy unit and the lack of other pollutants, natural gas is often considered a good transitional energy source [17, 18]. Furthermore, methane is important

as a raw material for other upgraded products [19, 20]. Therefore, methods to convert methane into a liquid, the most simple one being methanol, are highly desirable. These would allow storage at and transportation from various extractions sites, making this valuable resource accessible to the chemical industry, and, consequently, flaring would not be necessary. Being able to liquefy methane in biogas would also increase efficiency and less methane would slip into the atmosphere. Recent attempts to reduce the release of methane from cattle into the atmosphere has been performed in Denmark, where attempts to collect methane from cows have been made [21]. In addition to hydrocarbons, natural gas often contains large amounts of sulfur compounds, like H_2S [22, 23]. To remove this acidic sulfur compound (*sweetening* the sour natural gas), it would be necessary to oxidize methane with the sulfur compounds as the oxidant. However, to be able to do this, partial oxidation of methane is necessary. The alternative – complete oxidation – would give carbon dioxide, which is (to put it mildly) less useful.

Currently, industrial conversion of methane into methanol is a two-step process, where synthesis gas, or syngas (CO and H_2) is produced in an intermediate step, which is then converted into methanol or other chemicals [24]. This is very energy-intensive as it requires high pressures and temperatures at large, centralized plants, which is in sharp contrast to where the sources are. The alternative, and the outmost aim of this thesis, is to be able to efficiently and directly convert methane to methanol in one step. A challenge that puts catalytic research in the centre. Why? Because it is not only a question of finding a catalyst that increases the rate of a chemical reaction, but also a question of selectively steering the reaction to a desired product. More on the partial oxidation of methane can be found in chapter 4.

1.2 Catalysis

A catalyst is needed to selectively convert methane to, for instance, methanol. As already mentioned, a catalyst is a material that accelerates a chemical reaction, which may otherwise be slow or practically impossible, but is not consumed itself. The simplest way of looking at this is that the catalyst breaks and makes bonds within the reactants and offers a different pathway that facilitates the reaction at hand, see figure 1.1a).

Catalysis is not a foreign phenomena for most of us, and can be found in everyday examples such as in the aftertreatment system found in almost all vehicles, where dispersed noble metal catalysts clean the car exhaust from, amongst others, poisonous carbon monoxide and nitrogen oxides [27]. In chemical industry catalysis is used in almost all processes. The previously mentioned Haber-Bosch process use iron-based catalysts and has allowed for artificial fertilizers, which enhances food production and can sustain the global population. Zeolites, materials at the core of this thesis, are used to catalytically crack crude oil into shorter carbon chains like gasoline. These are examples of *heterogeneous catalysis* where the reactants and the catalysts are in different phases, here the catalysts are solids and the reactants gases or liquids. Other classes of catalysis are *homogeneous catalysis*, where both the reactants and the catalyst are in the same phase, often in solution, and *biocatalysis* – the solution of nature, with enzymes that often use shape selectivity of the substrates or the transition states to catalyze a reaction. Enzymes
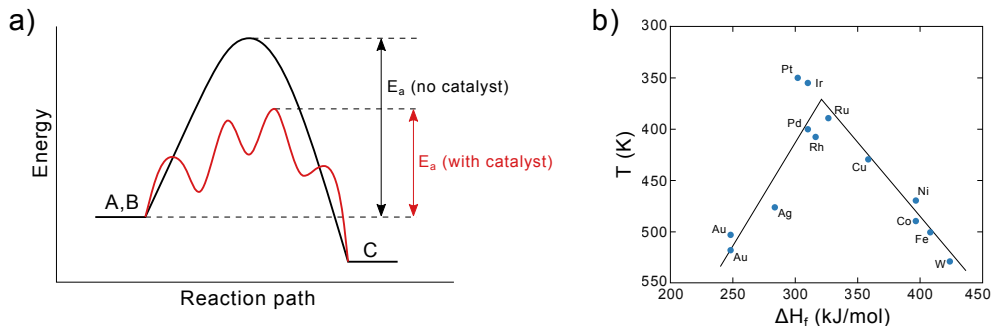
Figure 1.1: Illustration of how a catalyst a) presents an alternative reaction path to the same product. By binding reactants A and B, intermediate bonds and adsorbates are formed on the catalyst, which can then desorb and form the product C. In b) an illustration of the Sabatier principle and a volcano plot of the decomposition of formic acid on transition metals. Figures are adapted from Wikimedia Commons [25, 26].

are a common source of inspiration for the design of catalysts. The first mentioned example in the introduction, the fermentation of sugar to alcohol with the help of yeast, is an example of biocatalysis, where living yeast cells assist the reaction and reproduce at the same time [28, 29].

The concept of *active site*, specific groups of atoms that are responsible for most of the activity on heterogeneous catalyst surfaces, is central in catalysis and is crucial for our understanding and the rational design of new catalytic materials. Another governing concept in catalysis is the Sabatier principle, which states that there is an optimum in activity for a certain catalytic reaction when the interaction between adsorbates and catalyst is neither too strong, in which case the catalyst is poisoned or deactivated, nor too weak so the reaction never happens[2] [30, 31]. This is often illustrated in a volcano plot where the catalytic activity is plotted against a descriptor of the reaction. One example of this is the decomposition of formic acid on different transition metal catalysts where the heat of formation of the formate salt intermediate, ΔH_f, is used as a descriptor, see figure 1.1b). The temperature at which the reaction reaches a specific rate has an optimum when the interaction with the catalyst is neither to strong, nor to weak. The best performance is obtained for metals in the platinum group when the reaction temperature is lowest. For lower values of ΔH_f, adsorption is slow and limiting, and at higher values the desorption becomes rate-limiting and the catalyst poisoned. This is just one example of a descriptor of the reaction. Another, related, way of obtaining a descriptor is with the d-band model [32], which describe the volcano using the centre and filling of the d-electron band in the catalyst. A purely geometrical descriptor is the generalized coordination number [33–36], which links the geometry of a surface to its adsorption properties. To find the barrier of a reaction, it is possible to use Brønsted-Evans-Polanyi (BEP) relations [37, 38], which uses that the barrier often scales linearly with the initial and final states.

Finding scaling relations and descriptors for a catalytic reaction is one way to rationalize

---

[2]This is perfectly expressed with the Swedish word *lagom*.

catalytic activity. Finding large-scale trends and scanning over many catalytic materials, and thereby finding a better material and the next generation of catalysts, is the goal for many researchers.

1.3 Zeolites - a porous choice

"
At förekomma vidlyftiga epitheta, som medföra hvarjehanda olägenheter, och namn, som innebära någon egenskap, gemensam med flera arter, tager man sig dristighet, at kalla denna utan avsigt, Zeolites." [3]

– Axel Fredrik Cronstedt [39]

Zeolites were first described in 1756 by Axel Fredrik Cronstedt [39]. He observed that they produced large amount of steam upon heating and he named them zeolites after the greek words *zeo*, meaning *to boil* and *lithos*, meaning *stone*. They are a porous silicon oxide material with a wide range of pore sizes and cages. In everyday life, zeolites are often found in laundry detergents where they help to soften hard water by removing Ca^{2+} ions and exchanging them with Na^+ [40–43]. The active sites in these materials are typically counter ions, which compensate for the net charge created when exchanging some silicon atoms with aluminium. Zeolites are one of the few systems that we know can partially oxidize methane. However, they suffer from low yields and a closed catalytic cycle has only recently been reported [44, 45]. There is an ongoing discussion concerning the nature of the active site for the methane-to-methanol reaction, *i.e.* its structure and composition, and there is yet no clear answer. A more extensive background on zeolites can be found in chapter 4.

1.4 Scope

The aim of this thesis is to use first-principles calculations and microkinetic modelling to gain further insight into partial methane oxidation. The first and foremost example of this is the direct conversion of methane to methanol in zeolites, mainly zeolites with copper as the counter ion. To further understand how methanol is formed and interacts with the copper ions and with the zeolite, vibrational signatures and adsorption energies are calculated for methanol and other adsorbates and compared to experimental infrared (IR) spectroscopy measurements and temperature programmed desorption (TPD) profiles. The further reaction of methanol to dimethyl ether (DME) is also studied, where acidity is used as a descriptor of the reaction. The partial oxidation of methane is also studied for molybdenum sulfide clusters where methane is oxidized with H_2S to CH_3SH, CH_3SCH_3, and H_2. These small systems enables studies of a broader reaction network, similar to the

---

[3]Rough translation from 18th century Swedish: "Anticipating epithets of great magnitude, which cause every kind of inconvenience, and names that imply any trait, common to several species, one takes boldness, calling it without intention, Zeolites."

one in zeolite, and the possibility of studying selectivity between different products in partial methane oxidation.

The main method used in this thesis is density functional theory (DFT). The basics of DFT are discussed in chapter 2. The way electronic structure results are connected to experimentally measurable quantities in this thesis, is through statistical physics and microkinetic modelling. This is discussed in more detail in chapter 3. The background and a summary of the most important results in the papers this thesis is based on, can be found in chapter 4. Conclusions and reflections on the results and the computational methods can be found in chapter 5.

Chapter 2

Electronic structure methods

> " The electron is a *theory* we use; it is so useful in understanding the way nature works that we can almost call it real."

> – Richard P. Feynman [46]

In this quote Richard Feynman raises an important point: all we have in the natural sciences are models of the real world. Models that often help us understand and rationalize the way nature works, but that are still only models. We should keep that in mind when we discuss scientific results and pay special attention to the approximations we make and to the postulates we assume. This is certainly true when working with computational catalysis and electronic structure calculations.

Electrons are naturally important in catalysis, as they determine bonding and weakening and strengthening of bonds as different atoms interact. Electronic structure methods are therefore a useful tool for unveiling the details of a catalytic reaction. As a complement to experiments, it can enhance our atomistic understanding of a catalyst and can be an aid in the rational design of new catalysts. The electronic structure methods used in this thesis are called *first principles* since they are based only on fundamental assumptions, like the Schrödinger equation, and everything is calculated and predicted from these assumptions.

This chapter will focus on density functional theory (DFT), which is a common tool in computational physics and chemistry. It is a way of calculating the energy of an electronic system given only the electronic density and the principles of quantum mechanics.

2.1   The electronic structure problem

A quantum mechanical system is defined through the stationary eigenvalue equation

$$\hat{H}\Psi = E\Psi, \tag{2.1}$$

where $\hat{H}$ is the Hamiltonian operator describing the system, and its eigenvalues E are the quantized energy levels of the system. The total wavefunction Ψ contains all information and properties of the system and is essential for a quantum mechanical description. For catalysis applications, the energy is the sought-after quantity. To find the energy, we need to find the wavefunction, or the electron density $n(\mathbf{r}) = |\Psi|^2$.

In the non-relativistic limit[1], equation (2.1) is the Schrödinger equation [47]. Since we know that the interaction between charged particles is given by the Coulomb interaction,

---

[1]The equation holds also in the relativistic limit, in the Dirac equation, with the proper form of the Hamiltonian and the wavefunction.

we can write down the Hamiltonian for the many-body system of N electrons and K nuclei (or ions) with atomic number Z_I [48, 49]

$$\hat{H} = -\sum_{i=1}^{N} \frac{\hbar^2}{2m_{\mathrm{e}}} \nabla_i^2 - \sum_{I=1}^{K} \frac{\hbar^2}{2M_I} \nabla_I^2 + \frac{1}{4\pi\epsilon_0} \sum_{i=1}^{N} \sum_{j>i} \frac{e^2}{|\mathbf{r}_i - \mathbf{r}_j|}$$
$$- \frac{1}{4\pi\epsilon_0} \sum_{I=1}^{K} \sum_{i=1}^{N} \frac{Z_I e^2}{|\mathbf{r}_i - \mathbf{R}_I|} + \frac{1}{4\pi\epsilon_0} \sum_{I=1}^{K} \sum_{J>I} \frac{Z_I Z_J e^2}{|\mathbf{R}_I - \mathbf{R}_J|}, \tag{2.2}$$

where m_{e} is the mass of the electron, M_I the mass of the nuclei, $\mathbf{R}_I$ the position of nuclei I, and $\mathbf{r}_i$ the position of the electron i. This looks rather complicated and, together with the antisymmetry constraint on the total wavefunction, is not straightforward to solve. It turns out that the stationary Schrödinger equation can only be solved analytically for one-electron systems, *e.g.* the hydrogen atom. To be able to tackle larger systems, approximations have to be made.

2.1.1 The Born-Oppenheimer approximation

The first approximation that is usually applied is to separate the wavefunctions of the nuclei and electrons,

$$\Psi_{\mathrm{tot}}(\mathbf{r}, \mathbf{R}) = \Psi_{\mathrm{el}}(\mathbf{r}, \mathbf{R}) \Psi_{\mathrm{nucl}}(\mathbf{R}), \tag{2.3}$$

which is known as the Born-Oppenheimer approximation [50]. This means that the electrons follow the movement of the nuclei and adapt to any change in the nuclei positions immediately, while remaining in the same stationary state. The nuclei can then be treated in a classical fashion, interacting with an average potential from the electrons[2]. Intuitively, this is justified by the fact that the nuclei are much heavier than the electrons, $M_I >> m_e$, and that they therefore move on different time-scales. This assumes, however, that the energy of the nuclei movement is smaller than the energy required to excite the electrons, keeping them in the same stationary state. This is typically true for molecules, insulators, and semi-conductors, where the electronic excitation energy typically is larger than the vibrational and rotational energy. For metals, however, the Fermi level cuts right through an electronic band, meaning that small electronic excitations can happen within the same band. What saves us in metals is that, at temperatures much below the Fermi temperature (which is typically thousands of degrees), the electronic excitations are limited to a small region around the Fermi level which has little effect on most sought-after properties [51].

With the Born-Oppenheimer approximation, we can now drop the ionic kinetic energy term and the ion-ion interaction term in the Hamiltonian and only consider the terms involving electrons

$$\hat{H}_{\mathrm{el}} = -\sum_{i=1}^{N} \frac{\hbar^2}{2m_e} \nabla_i^2 + \frac{1}{4\pi\epsilon_0} \sum_{i=1}^{N} \sum_{j>i} \frac{e^2}{|\mathbf{r}_i - \mathbf{r}_j|} - \frac{1}{4\pi\epsilon_0} \sum_{I=1}^{K} \sum_{i=1}^{N} \frac{Z_I e^2}{|\mathbf{r}_i - \mathbf{R}_I|}. \tag{2.4}$$

---

[2]Treating the nuclei classically is a common approximation, but is strictly speaking separate from the Born-Oppenheimer approximation.

If we denote the interaction of electron i with the nuclei, the external potential, $V_{\text{ext}}(\mathbf{r}_i)$ and use Hartree atomic units ($\hbar = m_e = e = 1/(4\pi\epsilon_0) = 1$), we can write the Hamiltonian as

$$\hat{H}_{\text{el}} = -\frac{1}{2}\sum_i \nabla_i^2 + \sum_i \sum_{j>i} \frac{1}{|\mathbf{r}_i - \mathbf{r}_j|} + \sum_i V_{\text{ext}}(\mathbf{r}_i). \qquad (2.5)$$

This problem is still intractable, and from here, there are essentially two ways of moving forward. One way is to assume that the wavefunction is a linear combination of one-electron wavefunctions that satisfy the antisymmetry constraint using a Slater determinant construction [52]. This is the basis for the Hartree-Fock method [53–58][3] and the foundation for many theories following thereafter [49]. These wavefunction-based methods are still computationally expensive to solve [59], since the exchange (the energy associated with fulfilling the antisymmetry constraint) is non-local and expensive to evaluate. A way of improving the description of the electronic system, starting from Hartree-Fock, is to use Møller-Plesset perturbation theory, first suggested by Christian Møller and Milton S. Plesset in 1934 [60]. The basic idea is to include the exact Hamiltonian, including the unoccupied orbitals, in a perturbative way, improving the description of the correlation energy. This is quite computationally expensive and can only be realistically applied to small systems of tens of atoms. It is, however, one of the least expensive ways of improving the Hartree-Fock description and is relatively accurate, since it typically recovers 80-90 % of the correlation energy [51].

An alternative to wavefunction-based methods is using the electron density instead of searching for the wavefunction.

2.1.2 Introducing the electron density

The idea of working with the electron density instead of the wavefunction has been around ever since 1927 when Thomas and Fermi independently introduced the idea [61, 62]. However, in 1927, it was without actually knowing that it was formally possible to only use the electron density to evaluate the energy of an electronic system. It was not until 1964 when Hohenberg and Kohn [63] proved that the external potential $V_{\text{ext}}(\mathbf{r})$ is uniquely determined by the ground state electron density $n_0(\mathbf{r})$ and that the energy can be written as a *functional* of the electron density $n(\mathbf{r}) = |\Psi|^2$, which is minimized by the ground state [64]. In other words, while the Schrödinger equation gives us a way to construct the density from the potential

$$V_{\text{ext}} \to \Psi \to n, \qquad (2.6)$$

the Hohenberg and Kohn theory tells us how to go from the density to the potential, and together with equation (2.6) to the wavefunction which describes everything in the system

$$n \to V_{\text{ext}} \to \Psi \qquad (2.7)$$

---

[3]A brief explanation to these references; Hartree was the first to propose a self-consistent theory in 1928 [53]. Slater [54] and Gaunt [55] independently extended the method by applying the variational principle in 1928. Later Slater [56] and Fock [57] pointed out that the Hartree method did not respect antisymmetry in 1930, to which Slater had found a solution in 1929 [52]. Finally Hartree proposed a corrected method in 1935 more suitable for numerical work [58].

Further Hohenberg and Kohn prove that there exists a density functional that, if minimized, gives the ground state energy. Now we know that we can work only with the density, which is much more efficient since the density contains fewer degrees of freedom than the wavefunction (N instead of $3N$) and mainly, since the energy evaluation is local in terms of the density and non-local in wavefunction theory[4]. So far we know that it should be possible to consider the electronic many-body problem in terms of the electron density to obtain the ground state energy by using the variational principle and self-consistent iteration. However, to be able to know how to do this, we need the work by Kohn and Sham [65].

2.2 The Kohn-Sham approach (Density functional theory)

One year after the Hohenberg-Kohn theorems, Kohn and Sham proposed an approach to evaluate the density functional [65]. They made the ansatz of an auxiliary system of independent particles with orbitals ψ_i whose density

$$n(\mathbf{r}) = \sum_{i=1}^{N} |\psi_i(\mathbf{r})|^2, \tag{2.8}$$

is the real density of the system. This allowed them to write the energy functional in a clever way, namely

$$E_{\mathrm{KS}}[n] = T_0[n] + \int n(\mathbf{r}) V_{\mathrm{ext}}[n(\mathbf{r})] \, \mathrm{d}\mathbf{r} + E_{\mathrm{H}}[n] + E_{\mathrm{xc}}[n], \tag{2.9}$$

lumping the difficult many-body effects together, *i.e.* what we miss when we go from the full many-body wavefunction Ψ to the independent one-particle orbitals ψ_i, and calling it *exchange-correlation* (xc). Part of why this is such a useful way of writing the energy is that the first term, the kinetic energy of the *non*-interacting electrons $T_0[n]$, is a large part of the energy and is easy to calculate. The second term we recognize as the interaction with the ions (let us from now on call it $E_{\mathrm{ext}}[n]$), and is also simple to calculate. The third term

$$E_{\mathrm{H}}[n] = \frac{1}{2} \int \int \frac{n(\mathbf{r}) n(\mathbf{r}')}{|\mathbf{r} - \mathbf{r}'|} \, \mathrm{d}\mathbf{r} \, \mathrm{d}\mathbf{r}', \tag{2.10}$$

is straightforward to solve. This Hartree term is a mean-field approximation, meaning that each electron feels an average effect from all the other electrons, including itself. By applying the very useful variational principle on the Kohn-Sham energy functional

$$\frac{\delta E_{\mathrm{KS}}}{\delta \psi_i^*(\mathbf{r})} = 0, \tag{2.11}$$

we can derive the Kohn-Sham equation for electron i

$$-\frac{1}{2} \nabla^2 \psi_i(\mathbf{r}) + \left[V_{\mathrm{ext}}(\mathbf{r}) + \int \frac{n(\mathbf{r}')}{|\mathbf{r} - \mathbf{r}'|} \, \mathrm{d}\mathbf{r}' + \frac{\delta E_{\mathrm{xc}}}{\delta n(\mathbf{r})} \right] \psi_i(\mathbf{r}) = \varepsilon_i \psi_i(\mathbf{r}). \tag{2.12}$$

---

[4]This is evident in the exchange integral, which keeps the one-electron orbitals and needs to be evaluated for all orbitals i and j (see eq. (2.18)), while the density-dependent expressions like the Hartree term only needs to be evaluated for the density (see eq. (2.10)).

This is an eigenvalue problem for the Kohn-Sham orbitals ψ_i and eigenvalues ε_i. Provided that we have the exact exchange-correlation functional this would give us the true density $n(\mathbf{r})$. It is important to point out that this transformation to an auxiliary system of one-particle orbitals, the Kohn-Sham orbitals ψ_i, is fundamentally different from the description of the many-body Schrödinger equation with the full many-body wavefunction Ψ and is made only to obtain the true density $n(\mathbf{r})$. The Kohn-Sham orbitals ψ_i and energies ε_i are mathematical constructions, and are not related to the "correct" wavefunction and have no strict physical meaning[5]. There are, however, some relations to the the real system. The eigenvalues are, for example, related to the total energy according to

$$E[n] = \sum_{i=1}^{N} \varepsilon_i - E_{\mathrm{H}}[n] - \int n(\mathbf{r}) V_{\mathrm{xc}}[n(\mathbf{r})]\, \mathrm{d}\mathbf{r} + E_{\mathrm{xc}}[n]. \tag{2.13}$$

Since the Hartree energy is calculated in terms of the total density and the Kohn-Sham equation is solved for electron i, electron i interacts with itself. This is what is known as the *self-interaction error*, and is something the exchange-correlation functional tries to correct for. In Hartree-Fock, this is not a problem since Hartree-Fock keeps the real wavefunctions of the electrons and electron i then only interacts with the other electrons, and not itself.

What a DFT implementation basically does is to solve the Kohn-Sham equations, *i.e.* solve the eigenvalue problem in equation (2.12), in a self-consistent way with an approximation to the exchange-correlation. Many implementations also employ methods that simplify the treatment of the electrons close to the nuclei, the *core electrons*. Various methods to deal with the core states exist, such as using ultrasoft pseudopotentials [66] or the projected augmented wave method [67–69].

2.3 Exchange-correlation functional

The exchange-correlation part of the energy functional contains the many-body features of the electronic system. The exchange originates from the antisymmetry constraint on the total wavefunction (which is known in wavefunction-based methods, like Hartree-Fock) and correlation is what remains. The exact exchange-correlation functional E_{xc} is unfortunately not known. There are, however, a wide range of functionals available using different approximations. These different categories of approximations were described by John Perdew [70] as a *Jacob's ladder*[6] which reaches from the Hartree world to the heaven of chemical accuracy. Climbing higher up the ladder hopefully increases the accuracy, while the computational cost definitely increase. Choosing an exchange-correlation functional and making some approximation(s) make some people call it density functional *approximation* rather than theory [71].

The simplest approximation, and the one originally used by Kohn and Sham, is the the local density approximation (LDA), where the exchange and correlation energy is

---

[5]Although they often give good understanding of the system.

[6]A reference to the biblical story of Jacob: *And he dreamed, and behold, there was a ladder set up on the earth, and the top of it reached to heaven; and behold, the angels of God were ascending and descending on it!* – Genesis 28:12

only dependent on the local density [65], *i.e.*

$$E_{\text{xc}}^{\text{LDA}} = \int n(\mathbf{r})\epsilon_{\text{xc}}[n(\mathbf{r}), \mathbf{r}] \, d\mathbf{r}, \tag{2.14}$$

where ϵ_{xc} is the exchange-correlation energy density of the homogeneous electron gas, which can be calculated with Monte Carlo methods [72]. Spin can can be taken into account in the local spin density (LSD) approximation [73, 74], *i.e.*

$$\epsilon_{\text{xc}}[n(\mathbf{r})] \longrightarrow \epsilon_{\text{xc}}[n_\uparrow(\mathbf{r}), n_\downarrow(\mathbf{r})]. \tag{2.15}$$

This is a reasonable first approximation for many systems [71], especially metals without d-electrons.

Perhaps the most commonly used exchange-correlation approximation is the next rung on the ladder, the generalized gradient approximation (GGA), where also the gradient of the electron density is taken into account [75, 76]

$$E_{\text{xc}}^{\text{GGA}} = \int n(\mathbf{r})\epsilon_{\text{xc}}[\nabla n(\mathbf{r}), n(\mathbf{r}), \mathbf{r}] \, d\mathbf{r}. \tag{2.16}$$

One popular GGA functional is the one proposed by Perdew, Burke, and Ernzerhof, the PBE functional [77]. However, there exists a wide range of GGAs [78].

The rung thereafter, often called meta-GGAs [79], contains semi-local functionals which incorporate the kinetic energy of the Kohn-Sham orbitals $\tau(\mathbf{r}) = \sum_{i=1}^{N} \frac{1}{2}|\nabla\psi_i(\mathbf{r})|^2$ or the second derivatives of the electron density $\nabla^2 n(\mathbf{r})$ into the exchange-correlation functional.

To improve the accuracy further, we would need to abandon the local or semi-local picture of the exchange-correlation and go to hybrid functionals[7], which mix *exact exchange* in the exchange-correlation functional [78],

$$E_{\text{xc}}^{\text{hybrid}} = E_{\text{xc}}^{\text{GGA}} + a\left(E_{\text{x}}^{\text{exact}} - E_{\text{x}}^{\text{GGA}}\right). \tag{2.17}$$

The exact exchange derives from Hartree-Fock theory and the indiscernible particles principle for fermions *i.e.* since the electrons are identical, exchanging particle i and j must give the same result, which gives the anti-symmetry constraint. The energy associated with this is [80]

$$E_{\text{x}}^{\text{exact}} = -\frac{1}{2}\sum_{i,j}\int\int\frac{\psi_i^*(\mathbf{r})\psi_j^*(\mathbf{r}')\psi_j(\mathbf{r})\psi_i(\mathbf{r}')}{|\mathbf{r}-\mathbf{r}'|} \, d\mathbf{r} \, d\mathbf{r}', \tag{2.18}$$

which has a similarity to the Hartree energy in DFT (2.10), but with i and j exchanged. Hybrid functionals are much more computationally demanding than GGAs or meta-GGAs as the exact exchange integration is non-local and in principle stretches over the entire system. The even higher rungs on Jacob's ladder deal more explicitly with the correlation part, *e.g.* the random-phase approximation [81–83]. These are, however, beyond the scope of this thesis.

---

[7]Or alternatively extending the GGA functionals and using a Hubbard approach [48] to penalize delocalization in a parametric approach.

2.3.1 van der Waals interaction

The lower rungs of the ladder, local and semi-local functionals, clearly miss the van der Waals interaction, as this interaction is non-local and long-range correlation by nature. Some meta-GGA functionals are able to capture van der Waals interaction at medium range [84]. Perhaps the most pragmatic way of dealing with van der Waals correction is the Grimme formalism [85], where a $1/r^6$ term is parametrized to effectively capture the van der Waals interaction (in analogy to the simple Lennard-Jones pair-potential [86, 87]). Recently, Tkatchenko and Scheffler [88] introduced a parameter-free van der Waals description where the $1/r^6$ coefficients are calculated from the density. A more stringent way to include this non-local, long-range interaction is with a response integral of the form

$$E_{\mathrm{c}}^{\mathrm{nl}} = \frac{1}{2} \int n(\mathbf{r}) \phi(\mathbf{r}, \mathbf{r}') n(\mathbf{r}') \, \mathrm{d}\mathbf{r} \, \mathrm{d}\mathbf{r}', \tag{2.19}$$

as introduced by Lundqvist *et al.* [89], where they put forth appropriate expressions for the kernel[8] $\phi(\mathbf{r}, \mathbf{r}')$. This formalism if often called vdW-DF.

One of the van der Waals functionals used in this thesis is the optB86b-vdW functional [90], which uses Becke-86 exchange [91], LDA correlation, and long-range van der Waals correlation according to the vdW-DF formalism,

$$E_{\mathrm{xc}} = E_{\mathrm{x}}^{\mathrm{GGA}} + E_{\mathrm{c}}^{\mathrm{LDA}} + E_{\mathrm{c}}^{\mathrm{nl}}. \tag{2.20}$$

Another semi-local functional that includes the contributions of the response integral in equation (2.19) is the fitted and trained bayesian error estimation functional (BEEF-vdW) [92].

2.4 Basis set

To solve the Kohn-Sham equations numerically, the orbitals are expanded in a basis set, *i.e.*

$$\psi_i = \sum_j c_{ij} \chi_j, \tag{2.21}$$

where χ_j are the basis functions. Inserting this into the Kohn-Sham equation

$$\sum_j c_{ij} \hat{H} |\chi_j\rangle = \varepsilon_i \sum_j c_{ij} |\chi_j\rangle, \tag{2.22}$$

and multiplying with $\langle \chi_k |$ from the left we obtain the secular equation,

$$\sum_j c_{ij} \langle \chi_k | \hat{H} | \chi_j \rangle = \varepsilon_i \sum_j c_{ij} \langle \chi_k | \chi_j \rangle \Leftrightarrow \hat{H}_{kj} C_j = \varepsilon_i S_{kj} C_j, \tag{2.23}$$

or in vector form

$$(\mathbf{H} - \varepsilon_i \mathbf{S}) \mathbf{C} = \mathbf{0}. \tag{2.24}$$

---

[8]Without specifying the form of this kernel it is not possible to distinguish this from the Hartree potential. However, since this is slightly beyond the scope of this thesis, I do not expand on this.

Here we have the matrix representation of the Kohn-Sham hamiltonian $\mathbf{H}$, the overlap matrix $\mathbf{S}$, the Kohn-Sham eigenvalues ε_i and the basis coefficients $\mathbf{C}$. This matrix problem is what is solved in a DFT software. In the following paragraphs, some different aspects of the choice of basis set will be discussed.

2.4.1   Real-space grid

Perhaps the most straightforward choice is to use a uniform real-space grid, as implemented in the GPAW software [68, 93]. A real-space basis can, however, be tricky since it can depend rather strongly on the position of the grid points. Therefore the energy will not decrease monotonously when the number of grid points is increased. One advantage is that parallelization is comparably easy in real space, which makes it possible to study large systems.

2.4.2   Local basis functions

Another commonly used basis set are local functions centred around each atom. There are different types of local basis functions including gaussian-type orbitals, slater-type orbitals, and numerical orbitals [49]. In general local basis function sets can offer reasonable accuracy for a small number of basis functions [94], and are generally computationally cheap. They also often give good chemical information about, for instance, bonding [95–98]. However, it is difficult to know the degree of convergence with respect to the basis set size, since different basis sets can be qualitatively different. Another possible drawback is the so-called basis set superposition error, which is a consequence of the non-zero overlap of basis functions around different atoms. In other words the overlap matrix is not just the identity matrix, $S_{kj} = \langle \chi_k | \chi_j \rangle \neq \delta_{kj}$. This means that two or more local basis functions around different atoms can describe the same region in space. This gives rise to Pulay forces that are straightforward, but tedious, to correct for [48, 99]. Furthermore, the basis set is often associated with a cut-off radius, where, if outside, the overlap between basis functions is not evaluated. In the DMol^3 software, numerical basis functions are used. They are considered to be of high quality and are supposed to minimize basis set superposition effects [100].

2.4.3   Plane-waves

When studying a periodic system, plane waves are a natural choice of basis set, owing to their inherent periodicity. The Vienna Ab-initio Simulation Package (VASP) [101, 102] is a plane-wave basis set code that has been used in this thesis. In this approach, the Kohn-Sham orbitals are written as a sum over plane-waves:

$$\psi_j = \sum_{\mathbf{k}} c_{j\mathbf{k}} e^{i\mathbf{k}\cdot\mathbf{r}}, \tag{2.25}$$

where the overlap is zero and $S_{ij} = \delta_{ij}$. This can be viewed as Fourier components to the Kohn-Sham orbitals, and by including plane-waves with a higher frequency, more rapidly varying features in the Kohn-Sham orbitals can be described. Therefore, the energy will

decrease monotonously with the number of plane-wave basis functions included[9]. In a plane-wave basis set approach, some operations are more readily evaluated in the reciprocal k-space, meaning that Fourier transforms back and forth are involved. This is often not a severe limitation, but becomes computationally expensive for large systems [68]. Another aspect of using plane-waves is the k-point grid that is needed to evaluate the integrals in reciprocal space. The system needs to be converged with respect to the number of grid points [103]. Since real space and reciprocal space are inversely proportional to each other, for the large computational cells relevant in this thesis, it is enough to only have one k-point. Further, plane-waves can only treat periodic systems. To describe molecules and systems without periodic boundary conditions with plane-waves, it is necessary to introduce enough vacuum in the computational cell to ensure that the system does not interact with itself. This makes plane-waves less efficient for non-periodic system since they describe all regions of space, also the vacuum around the system of interest, which is associated with some cost.

---

[9]Assuming enough plane-waves initially so the energy is decently described.

Chapter 3

Atomistic modelling of catalytic reactions

> "
> With great computational power comes great chemical accuracy."

– Mikael Valter [104]

Computational methods, as described in the previous chapter, can give the energy of a given configuration of atoms. To be able to describe reactions on surfaces it is also necessary to find the reaction path and their barriers. It is necessary to be able to include entropy and temperature effects, and to be able to connect all of this to measurable properties and compare with experiments.

This chapter is meant to give an overview of how the results from DFT can be expanded upon and connect to the macroscopic world.

3.1   Identifying the active site and reaction intermediates

The concept of *active site*, was first put forth in 1925 by Hugh Stott Taylor [105] who realized that not all atoms on a catalyst surface are *active* in a reaction. In zeolites, which will be a main topic in the following chapter, the active site usually consists of exchange ions, external to the framework atoms, but inside the pores or cages of the zeolite.

First we need to identify a possible candidate for the active site. Once an active site has been identified, we need to pick a reasonable reaction mechanism, which will guide how different reaction intermediates should be placed on or around the active site. All of the above is usually done on the basis of chemical intuition. Comparing to previous work or experience, we guess the structure of reaction intermediates. Then, we simply relax this to the closest local minimum in the potential energy landscape.

3.2   Calculating forces

To be able to relax a system to the closest local minimum in the potential energy landscape, we minimize the forces in the system. As in classical mechanics, the force is defined as minus the gradient of the potential. In an atomic system, the force on atom I is thus

$$\mathbf{F}_I = -\frac{\partial E}{\partial \mathbf{R}_I}. \tag{3.1}$$

To calculate the gradient of the energy, we use the often called Hellmann-Feynman theorem[1] [106, 107], which states that if the Hamiltonian depends on a parameter λ, the energy derivative is

$$\frac{\partial E_\lambda}{\partial \lambda} = \langle \Psi_\lambda | \frac{\partial \hat{H}_\lambda}{\partial \lambda} | \Psi_\lambda \rangle. \tag{3.2}$$

When λ is the coordinate of the nucleus of atom I, the force on atom I is [108]

$$\mathbf{F}_I = -\langle \Psi | \frac{\partial \hat{H}_\lambda}{\partial \mathbf{R}_I} | \Psi \rangle = \int n(\mathbf{r}) \frac{Z_I(\mathbf{r} - \mathbf{R}_I)}{|\mathbf{r} - \mathbf{R}_I|^3}\, \mathrm{d}\mathbf{r} + \sum_{J \neq I} \frac{Z_I Z_J(\mathbf{R}_I - \mathbf{R}_J)}{|\mathbf{R}_I - \mathbf{R}_J|^3}, \tag{3.3}$$

assuming that the Born-Oppenheimer approximation holds. Since this only depends on the electron density $n(\mathbf{r})$ and the positions of the nuclei, this means that both the energy and forces can be calculated in a single-point calculation. Once the energy and density are found for a certain atomic structure, the closest ground state of the atomic structure can be obtained by moving the atoms along the forces, using for instance a Quasi-Newton method [109]. Therefore, calculating the forces allows to find the intermediates in the considered reaction mechanism.

3.2.1 Analytical second derivative

The analytical expression for the second derivative is also attainable using the Hellmann-Feynman theorem as [110]

$$\begin{aligned} \frac{\partial^2 E_\lambda}{\partial \lambda^2} &= \langle \Psi_\lambda | \frac{\partial^2 \hat{H}_\lambda}{\partial \lambda^2} | \Psi_\lambda \rangle + 2 \langle \frac{\partial \Psi_\lambda}{\partial \lambda} | (E_\lambda - \hat{H}_\lambda) | \frac{\partial \Psi_\lambda}{\partial \lambda} \rangle \\ &= \langle \Psi_\lambda | \frac{\partial^2 \hat{H}_\lambda}{\partial \lambda^2} | \Psi_\lambda \rangle + 2 \langle \Psi_\lambda | \frac{\partial(\hat{H}_\lambda - E_\lambda)}{\partial \lambda} | \frac{\partial \Psi_\lambda}{\partial \lambda} \rangle, \end{aligned} \tag{3.4}$$

which involves computing the derivatives of the wave-function and thereby the basis functions. In wave-function theory, like Hartree-Fock, this is often used to calculate the second derivative with respect to the nuclear coordinates, while in Kohn-Sham DFT, this is usually not the case.

3.3 Calculating vibrational frequencies

Describing vibrations in a system is crucial to be able to include entropy and temperature effects in the reaction mechanism. Vibrations are small movements, deviations from the equilibrium positions of the atoms. Frequencies for these vibrations are often calculated in a perturbative manner, by expanding the potential around the equilibrium position $\mathbf{r}_0$, and truncating at the second order. The expression of the potential is then [111, p. 520]

$$V(\mathbf{r}) = V(\mathbf{r}_0) + \sum_i \frac{\partial V}{\partial r_i}\bigg|_{\mathbf{r}_0} \Delta r_i + \frac{1}{2} \sum_{i,j} \frac{\partial^2 V}{\partial r_i \partial r_j}\bigg|_{\mathbf{r}_0} \Delta r_i \Delta r_j + ... \tag{3.5}$$

---

[1]Which is slightly unfair, since Ehrenfest in 1927, Born and Fock in 1928, Güttinger in 1932, and Pauli in 1933 independently treated the same thing before Hellmann in 1937 and Feynman in 1939 [48].

where the first term is a constant and will just shift the energy scale and the first order derivative is by definition zero since $\mathbf{r}_0$ is the equilibrium position. The second order derivative is the harmonic term, and the expansion is generally truncated after this term. Sometimes, it is a necessary improvement to include higher-order terms, and include anharmonic effects, for instance, when modelling thermal transport, which includes dissipation [112]. Including higher-order terms is, however, computationally costly since it requires many more energy evaluations.

To evaluate the potential energy landscape $V(\mathbf{r})$, electronic structure calculations are a natural choice. It is, of course, also possible to use a model potential to calculate the energy for the different displacements. However, a model potential is usually trained for a specific system and to describe a specific quantity. To have transferability, it therefore is preferable to use an electronic structure method. In Kohn-Sham DFT, the second derivatives are generally evaluated with finite differences rather than using the analytical expression of the second derivative in section 3.2.1. The second derivatives are thereby calculated by displacing each atom and calculating the forces on each atoms, *i.e.*

$$\Delta V\left(\mathbf{r}\right) \simeq \frac{1}{2}\sum_{i,j} \left.\frac{\partial^2 V}{\partial r_i \partial r_j}\right|_{\mathbf{r}_0} \Delta r_i \Delta r_j = -\frac{1}{2}\sum_{i,j} \left.\frac{\partial F_i}{\partial r_j}\right|_{\mathbf{r}_0} \Delta r_i \Delta r_j. \tag{3.6}$$

By evaluating these changes in the forces, the resulting Hessian matrix can be diagonalized and the eigenvalues will correspond to the harmonic frequencies squared, in analogy to the quantum harmonic oscillator [64]

$$\hat{H}_i = -\frac{1}{2}\frac{\partial^2}{\partial y_i^2} + \frac{1}{2}m\omega_i^2 y_i^2, \tag{3.7}$$

where y_i are the eigenmodes. Having the eigenfrequencies ω_i, the eigenenergies can be obtained as

$$E_{i,n} = \hbar\omega_i \left(n + \frac{1}{2}\right), \quad n = 0, 1, 2, ... \tag{3.8}$$

and the corresponding eigenvector will be the vibrational mode. This estimation of the vibrational frequencies of a system is very useful when interpreting infrared spectroscopy measurements and for calculating vibrational free energies and entropies.

3.4   Finding transition states

On empirical grounds, Svante Arrhenius in 1889 proposed an equation for the temperature dependence of the rate constant of an elementary reaction, the so-called Arrhenius equation [31, 113, 114]

$$k = A\, e^{-E_{\mathrm{a}}/k_{\mathrm{B}}T}. \tag{3.9}$$

In this equation E_{a} is the energy required to overcome the activation barrier. Empirically, this can be obtained through measuring the activity of a reaction as a function of temperature and making an Arrhenius plot of $\log k$ versus T^{-1}, in which the slope is $-E_{\mathrm{a}}/k_{\mathrm{B}}$. However, experimentally, it is very difficult to know which elementary steps are
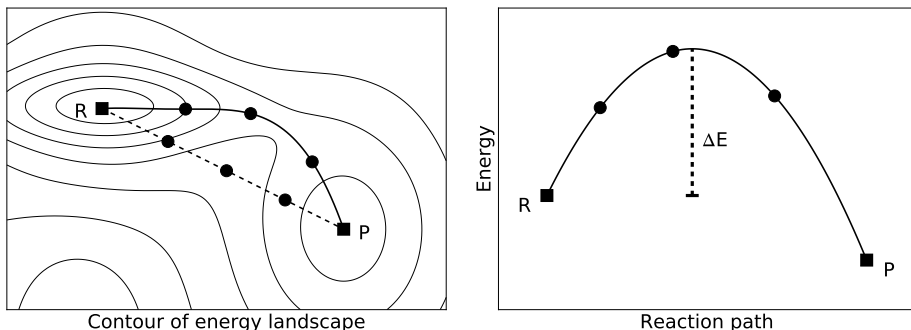
Figure 3.1: Illustration of the nudged elastic band method. To the left, an initial guess (dashed) for the reaction path and then the final path over the saddle point (solid) is found with a series of minimizations perpendicular to the reaction path. To the right, the energy profile along the minimum energy path.

important. In order to model each elementary step, we somehow need to be able to find the energy barrier for each step.

The lowest energy barrier between a reactant and a product, say R and P, is found over a ridge or a saddle point in the energy landscape, having a negative gradient only in one direction, along the reaction path. It is necessary to find this saddle point, or *transition state*, to calculate the kinetic rate. To find reaction barriers and transition states it is common to use a nudged elastic band (NEB) algorithm, or the improvement climbing image NEB [115–117]. The idea behind the NEB method is to first construct a series of images that connect the R and P, by, for example, interpolating the coordinates linearly between the two states. By coupling the images with spring forces along the reaction coordinate, and minimizing the forces perpendicular to this direction, the lowest energy path will be found[2] (see figure 3.1 for an illustration). The climbing image NEB algorithm will move the image closest to the saddle point closer to the maximum, by moving it in the opposite direction of the maximum force. To confirm that the obtained transition state truly is a saddle point, a vibrational analysis needs to be performed. If it is a saddle point, there will be one frequency that is imaginary, which corresponds to a negative second derivative along that eigenmode.

An alternative to the NEB method is the *dimer* method [118, 119], which only uses two images that are moved to the nearest saddle point through a series of translations and rotations. Yet another method for finding transitions states is the Linear Synchronous Transit (LST) [120] where the reaction path is constructed by interpolating between reactants and optimized orthogonally to the reaction path. LST is used in the DMol^3 software together with a Quadratic Synchronous Transit (QST) method that uses three structures to interpolate the reaction path.

If a transition states can be well described in terms of broken and formed bonds, as is often the case in zeolite-catalysed reactions, it is possible to define a linear combination of these bonds as a constrained coordinate. By scanning over this constrained coordinate,

---

[2]Or to be more precise, the lowest energy path closest to the initial guess will be found.

letting everything but this constraint relax, it is possible to find a transition state. This is used in the Automated Relaxed Potential Energy Surface Scans (ARPESS) package [121].

3.5   The statistical picture

A statistical treatment of the catalytic system is needed to model a chemical reaction from first principles. Statistical physics, or statistical mechanics, describes a microscopic way of thinking about thermodynamics. Everything is based on the number of ways a system can be arranged in *microstates*, and it is a powerful way of connecting energies and electronic structure calculations to macroscopic quantities and behaviours. The fundamental assumptions of statistical physics is that all microstates are equally probable in a closed system with constant energy (U), volume (V), and number of particles (N). The probability of finding such a system in a non-degenerate microstate is

$$\mathcal{P} = \frac{1}{W},$$ (3.10)

where W is the total number of microstates. For a system degenerate by Ω the probability is

$$\mathcal{P}(\Omega) = \frac{\Omega}{W}.$$ (3.11)

This is why all particles in the air do not all gather in one corner of the room; there are just so many more ways of distributing the particles evenly throughout the room [122]. The quantity that governs the physics in this ensemble is the entropy, defined through

$$S = k_{\mathrm{B}} \ln \Omega.$$ (3.12)

The most probable configuration is that with the highest entropy, or the largest degeneracy Ω.

In reality, however, it is more likely that the temperature is constant, rather than the energy. This can be taken into account by connecting the system to a large reservoir that can exchange energy with the system, and thereby keep the temperature constant. In such a system, with constant temperature (T), volume (V), and number of particles (N), the probability of a state is given by the Boltzmann distribution

$$\mathcal{P}(s) = \frac{e^{-E(s)/k_{\mathrm{B}}T}}{\sum_{s} e^{-E(s)/k_{\mathrm{B}}T}} = \frac{e^{-E(s)/k_{\mathrm{B}}T}}{\mathcal{Z}},$$ (3.13)

where $E(s)$ is the energy of the system, k_{B} is Boltzmann's constant, and the sum over states[3] $\mathcal{Z}$ is the canonical partition function. The physics in this ensemble is governed by the Helmholtz free energy

$$F = -k_{\mathrm{B}} T \ln \left(\mathcal{Z} \right),$$ (3.14)

and the most probable state is the state with the lowest free energy.

---

[3]Zustandssumme in German.

Often it is easier to keep the pressure constant, rather than the volume, and in such a Gibbs ensemble with constant temperature, pressure (p), and number of particles (N), the free energy is given by $G = F + pV$. When contemplating relative free energies from a computational perspective, the volume change is often negligible and $\Delta G \approx \Delta F$ [123], at least when considering different adsorbed intermediates.

All of this connects to quantum mechanical calculations through the energy. Given a set of energies for different configurations $E(s)$, arrangements of atoms *et cetera*, we can calculate the free energy and thereby determine which configuration is more probable.

3.5.1 Partition functions of adsorbates

Considering an adsorbed molecule on a catalyst's surface, the partition function can be written as a product of the various separable degrees of freedom

$$\mathcal{Z} = Z_{\text{trans}} Z_{\text{vib}} Z_{\text{rot}} Z_{\text{elec}} Z_{\text{nucl}}. \tag{3.15}$$

Since we are interested in reactions on surfaces, going from an adsorbed reactant R to a product P, it is unlikely that the sum over the nuclei states will change. We will therefore focus on the other terms.

The most common expression for the translational partition function is derived from the ideal gas where the particles have kinetic energy $E = \mathbf{p}^2/2m$. In the one-dimensional case, the partition function can then be written as an integral[4] over all positions and momenta

$$Z_{\text{trans}}^{\text{1D}} = \frac{1}{h} \int\limits_0^l \mathrm{d}x \int\limits_{-\infty}^{\infty} e^{-p_x^2/2mk_\text{B}T} \, \mathrm{d}p_x = l \frac{(2\pi m k_\text{B}T)^{\frac{1}{2}}}{h}. \tag{3.16}$$

In three dimensions the partition function is generalized to

$$Z_{\text{trans}}^{\text{3D}} = V \frac{(2\pi m k_\text{B}T)^{\frac{3}{2}}}{h^3} = \frac{V}{\Lambda^3}, \tag{3.17}$$

where Λ is the thermal wavelength (the de Broglie wavelength), and is just a convenient way of writing the partition function.[5] The characteristic dimension l or V is the length or volume in which the particle moves. Volume is often less straightforward to use than the pressure of a gas. In many cases, it is a good approximation to connect V and the pressure p through the ideal gas law

$$\frac{\mathcal{V}}{N} = \frac{k_\text{B}T}{p}, \tag{3.18}$$

where $\mathcal{V}$ is the total volume for all particles N.

Assuming a harmonic potential around the local minima in the potential energy surface, the vibrational energies are those of the quantum harmonic oscillator:

$$E_{i,n} = \hbar \omega_i \left(n + \frac{1}{2} \right), \quad n = 0, 1, 2, \dots \tag{3.19}$$

---

[4]Since phase space can be divided into small cells with side h.

[5]There is, however, an assumption that $V/\Lambda^3 \gg 1$ behind all this, *i.e.* that the wavelength of the particle must be much smaller than the length of the container in which it is confined.

Using these energies in the partition function, we obtain

$$Z_{\text{vib}} = \sum_{n=0}^{\infty} e^{-\hbar\omega_i\left(n+\frac{1}{2}\right)/k_\text{B}T} = \frac{e^{-\frac{1}{2}\hbar\omega_i/k_\text{B}T}}{1 - e^{-\hbar\omega_i/k_\text{B}T}}, \qquad (3.20)$$

where the nominator is the zero-point energy (the energy for $n = 0$).

Rotations of molecules are essentially treated in the same way. From the energy levels of rotation, assuming a rigid rotor and that the distance between the atoms is fixed[6], the partition function for a polyatomic molecule can be written as [31, p. 92]

$$Z_{\text{rot}} = \frac{1}{\sigma} \left(\frac{8\pi^2 k_\text{B}T}{h^2}\right)^{\frac{3}{2}} \sqrt{\pi I_A I_B I_C}, \qquad (3.21)$$

where I_A, I_B, and I_C are the moments of inertia along the three principal axes, and σ is the symmetry factor, an orientational degeneracy. For the molecules studied in this thesis the symmetry number is $\sigma = 1$ for methanol and molecules with no orientational degeneracy, 12 for methane (it is possible to rotate it in many ways and obtain the same structure), and 2 for homonuclear diatomic molecules [124, p. 162]. For methane, the translational partition function $Z_{\text{trans}} \approx 8 \cdot 10^6$ at $200\,^{\circ}\text{C}$ and $1\,\text{atm}$, the rotational $Z_{\text{rot}} \approx 70$, and the vibrational $Z_{\text{vib}} \approx 1$, which illustrates that the translational degrees of freedom have the largest contribution to the entropy and free energy for a gas-phase molecule.

Often we consider adsorbed species to have only vibrational degrees of freedom, while any rotations or translations are well described as frustrated vibrations in a harmonic potential. If this is not the case, there are ways around it. One different approach is to assume that the adsorbates are free to move along the surface, using a two-dimensional ideal-gas expression for the partition function. If there is a small diffusion barrier between two sites, this can be taken into account with the partition function for a hindered translation [125]. Another rigorous approach is to sample the energy surface along the surface by moving the adsorbates systematically and the partition function can be calculated by integrating over the energy surface. A recent paper by Jørgensen and Grönbeck compares these different approximations for CO oxidation over Pt(111) [126].

3.6 Microkinetic modelling - connecting to catalytic reactions

One common way of connecting calculated microscopic quantities, such as energies, structures, and vibrational frequencies to macroscopic quantities, *e.g.* turn-over frequencies, is by constructing a microkinetic model that describes the reaction rates between reactants, intermediates, and products. This tells us something about the time evolution of a system, which steps are important, and lets us extract measurable quantities such as apparent activation energies, turn-over frequencies, and kinetic bottlenecks.

---

[6]It would complicate things considerably if we do not, and it will only result in a small correction.

3.6.1 Transition state theory

Instead of resolving all energetic states as a function of all the positions and momenta of all particles, the time evolution of a reaction is often modelled as hopping between different local minima, across a saddle point in the free energy landscape. The probability of observing the system in a certain state α must then be written down as a gain-loss relation often called the Master Equation [127]:

$$\frac{\mathrm{d}\mathcal{P}_\alpha}{\mathrm{d}t} = \sum_\beta \left[W_{\beta \to \alpha} \mathcal{P}_\beta - W_{\alpha \to \beta} \mathcal{P}_\alpha \right], \tag{3.22}$$

where $W_{\alpha \to \beta}$ is the transition frequency for jumping from state α to state β, and $\mathcal{P}_\alpha$ is the probability of the system being in state α. A common approximation is to consider an average system with a large number of sites and a uniform distribution of adsorbates, in a mean-field approximation. The probability of being in the state α is then given by the average concentration (often coverage) of α, often denoted θ_α.

Now we only need an expression for the transition frequency. In conventional transition state theory (TST) [128, 129], a reaction is considered to proceed from a reactant R through an activated reaction intermediate $R^\ddagger$, called a transition state (TS), to a product P. The reactant state and the transition state are assumed to obey Boltzmann statistics and recrossing the energy landscape once the transition state has been crossed is not allowed [130]. This can be summarized as

$$R \rightleftarrows R^\ddagger \to P. \tag{3.23}$$

However, relabelling R and P, the transition frequency in the other direction can be obtained.

Considering a reaction through a transition state, the frequency at which a chemical reaction happens can be expressed as

$$W_{R \to P} = \nu \frac{\mathcal{P}(R^\ddagger)}{\mathcal{P}(R)} = \nu \frac{\mathcal{Z}^\ddagger}{\mathcal{Z}} = \frac{k_{\mathrm{B}} T}{h} \frac{\mathcal{Z}^\ddagger}{\mathcal{Z}}. \tag{3.24}$$

The ratio between the sums of available states for R and $R^\ddagger$, given by the partition functions, gives the probability of being in the activated reaction intermediate compared to the reactant. The trial frequency ν is generally considered to be the frequency of the *reaction coordinate*, which is the vibration crossing the saddle point between R and P. In the classical limit, assuming $h\nu >> k_{\mathrm{B}}T$, it can be proven that the trial frequency equals $k_{\mathrm{B}}T/h$, which at least dimensionally is a frequency. See for example [31, 130] for further details. The reaction coordinate is along one degree of freedom, so $\mathcal{Z}^\ddagger$ has one degree of freedom less.

Separating out the electronic part and expressing the partition function with reference to the local energy minima, the transition rate can be expressed as

$$W_{R \to P} = \frac{k_{\mathrm{B}} T}{h} \frac{\mathcal{Z}'^\ddagger}{\mathcal{Z}'} e^{-\Delta E / k_{\mathrm{B}} T} \equiv k_{\mathrm{TST}}, \tag{3.25}$$
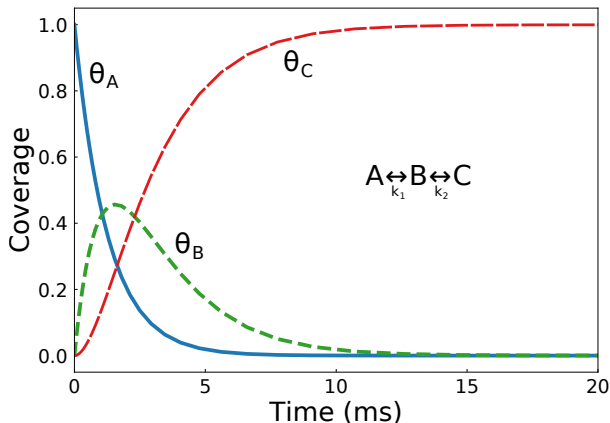
Figure 3.2: Example of the time-dependent solution for a linear A $\leftrightarrow$ B $\leftrightarrow$ C reaction. Here the rate constants are $k_1^{\rightarrow}$=800 s^{-1}, $k_1^{\leftarrow}$=1 s^{-1}, $k_2^{\rightarrow}$=500 s^{-1}, and $k_2^{\leftarrow}$=0.1 s^{-1}

where ΔE is the energy barrier between the transition state and the reactant[7]. This is how the TST rate coefficient is expressed, we "only" need to calculate the partition functions for the transition state $R^{\ddagger}$ and the different reaction intermediates R and P to get the forward and backward rate constants.

3.6.2 Putting the pieces together

Now that we have a way of expressing the reaction rates, we can briefly discuss how to put it all together. First of all, we will need a reaction mechanism. This can be simple and linear, $A + B \rightarrow AB$ for instance, in which case the gain-loss equation corresponding to the change in concentration of A would be

$$\frac{\mathrm{d}\theta_A}{\mathrm{d}t} = k_{A+B \rightarrow AB}\theta_A\theta_B - k_{AB \rightarrow A+B}\theta_{AB}, \tag{3.26}$$

or much more complex with different side reactions and cycles. If A is adsorbed on a surface, θ_A is often called the fractional coverage of A, and is a number between 0 and 1. Notice that the probability of A meeting B and forming AB is proportional to the concentration of A times the concentration of B, $\theta_A\theta_B$; this is the *law of mass action* and within a mean-field approximation. If we have a more complicated reaction mechanism, it is then "just" a matter of keeping track of all reactions and coverages when putting together the loss-gain equations. An example of the time evolution obtained from solving the loss-gain equations numerically is shown in figure 3.2. Here the sequential reaction $A \leftrightarrow B \leftrightarrow C$ is considered, starting from only A species. We see an initial transient behaviour, where there is a coverage of species B, which eventually turns into a steady-state coverage of C, when the time-derivative of all coverages reaches zero. In this simple example the rate constants are $k_1^{\rightarrow}$=800 s^{-1}, $k_1^{\leftarrow}$=1 s^{-1}, $k_2^{\rightarrow}$=500 s^{-1}, and $k_2^{\leftarrow}$=0.1 s^{-1}.

---

[7]and a positive number.

An important feature of a system like this is that the values of the rate constants determine the time-scale(s) of the system. The time necessary to reach steady-state is of the same order of magnitude as the inverse of the slowest rate constant. For numerical purposes it can be good to also sample the shortest time scales, which is given by the inverse of the fastest rate constant.

3.6.3 Gas-phase adsorptions

Another aspect we need to be aware of is how to model gas-phase adsorptions, especially non-activated adsorption. One way to model adsorption is to consider that the molecule goes from a three-dimensional gas to a two-dimensional gas on the surface, and that there is no barrier $\Delta E = 0$, $i.e.$

$$k_{\mathrm{ads}} = \frac{k_{\mathrm{B}}T}{h} \frac{\mathcal{Z}_{\mathrm{trans}}^{\mathrm{2D}}}{\mathcal{Z}_{\mathrm{trans}}^{\mathrm{3D}}} = \frac{k_{\mathrm{B}}T}{h} \frac{l^2}{\Lambda^2} \frac{\Lambda^3}{l^3} = \frac{k_{\mathrm{B}}T}{h} \frac{A}{\Lambda^2} \frac{p\Lambda^3}{k_{\mathrm{B}}T} = \frac{p\,A}{\sqrt{2\pi m k_{\mathrm{B}}T}}, \qquad (3.27)$$

where we used the ideal gas law $l^3 = V = k_{\mathrm{B}}T/p$, and $l^2 = A$ is the characteristic area in which the adsorbed molecule moves. Here we have assumed that all molecules approaching the surface successfully adsorb. Generally, an adsorption is not always successful and can depend on the orientation of the molecule as it approaches, where on the surface the molecule hits et $cetera$. This is often introduced in an efficiency coefficient, or $sticking$ $coefficient$ [31, 130]. Putting the sticking coefficient to one, as we implicitly did above, gives an upper limit of the rate of adsorption. It should be noted that this is only one way of modelling adsorption. It is not necessary to assume the adsorbed molecule to be a two-dimensional gas that can move freely along the surface. Another possibility is to assume that the molecule sticks to one site and does not move around, or that it has a small diffusion barrier and use expressions for a hindered translator.

The desorption rate, $i.e.$ the backward rate, can be defined through the fact that

$$\frac{k_{R \to P}}{k_{P \to R}} = \frac{\mathcal{Z}^{\ddagger}/\mathcal{Z}_R}{\mathcal{Z}^{\ddagger}/\mathcal{Z}_P} = \frac{\mathcal{Z}_P}{\mathcal{Z}_R} = e^{\ln \mathcal{Z}_P - \ln \mathcal{Z}_R} = e^{-\Delta G/k_{\mathrm{B}}T}, \qquad (3.28)$$

where ΔG is the free energy difference between the product and reactant state. This is also called the $equilibrium$ $constant$ K_{eq}. This means that we can calculate the desorption coefficient as

$$k_{\mathrm{des}} = k_{\mathrm{ads}} \frac{\mathcal{Z}_{\mathrm{G}}}{\mathcal{Z}_{\mathrm{A}}}, \qquad (3.29)$$

where $\mathcal{Z}_{\mathrm{A}}$ is the partition function for the adsorbed state, and $\mathcal{Z}_{\mathrm{G}}$ for the system with the gas-phase species.

From an implementation point of view, the question of how to define the desorption if there is no back-adsorption (consider for example a flow reactor where the products are continuously being removed) can be difficult. Should the desorption event be a function of the pressure dependent adsorption (which does not exist) or not? There is a way around this, by rewriting the partition function for the desorbed state as

$$\mathcal{Z}_{\mathrm{G}} = Z_{\mathrm{surface}}\, Z_{\mathrm{gas,trans}}\, Z_{\mathrm{gas,rot}}\, Z_{\mathrm{gas,vib}}, \qquad (3.30)$$

where we look at the separate parts for the empty surface and the gas-phase molecule. Plugging this into equation (3.29) and using the known expressions for $Z_{\text{gas,trans}}$ and k_{ads}, we get

$$k_{\text{des}} = \frac{\Lambda}{h} \, p \, A \frac{k_{\text{B}}T}{p\Lambda^3} \frac{Z_{\text{surface}} \, Z_{\text{gas,rot}} \, Z_{\text{gas,vib}}}{Z_{\text{ads,vib}}} e^{-\Delta E/k_B T} \tag{3.31}$$

$$= \frac{k_{\text{B}}T}{h} \frac{A}{\Lambda^2} \frac{Z_{\text{surface}} \, Z_{\text{gas,rot}} \, Z_{\text{gas,vib}}}{Z_{\text{ads,vib}}} e^{-\Delta E/k_B T}, \tag{3.32}$$

where ΔE is the energy difference between the adsorbed and desorbed systems. This is, from an implementation point of view, much more useful since it is pressure independent.

3.6.4 The mean-field approximation

An observant reader might have noticed that the mean-field approximation was used in equation (3.26) without much justification. The mean-field approximation assumes that all adsorbed species are randomly distributed on the catalytic surface and that there is no interaction between the adsorbed species [31]. If there is lateral interactions (especially attractive interactions) between adsorbates, the rate of A reacting with B is not just $\theta_A \theta_B$, as assumed in section 3.6.2. The alternative to using a mean-field model is to perform a fully stochastic kinetic Monte Carlo simulation [127].

For catalysts with isolated sites (like zeolites which will be introduced in the next chapter), the distance to the neighbouring sites is large and the interaction weak, and the sites can be treated independently. For these systems, the mean-field approximation should work and the mean-field coverages θ_i correspond to the fractional number of sites of each intermediate i. As a first approximation, for the molybdenum sulfide clusters, we have used a mean-field kinetic model, even though there are lateral interactions. In principle it would be necessary to turn to a kinetic Monte Carlo to model the lateral interactions. Some lateral interactions are implicitly included in the energy calculations. Another potentially cumbersome feature of these small clusters is that they are probably too small to have linear scaling of adsorption energies when different adsorbates are adsorbed on different sites. This would mean calculating all possible combinations of adsorbates on all cluster, which would be a time-consuming and extensive task.

3.6.5 Degree of rate control

Given a net rate of a reaction, *i.e.* how many times per second a product is produced, we can perform a sensitivity analysis to attempt to unravel the behaviour of the reaction. One way to do this is to perform a *degree of rate control* analysis, as proposed by Campbell *et al.* [131, 132]. In this scheme, the rate coefficients k_i (or equivalently the barriers) are changed and the response of the total rate r is examined. In a normalized way, this corresponds to

$$X_{\text{RC},i} = \frac{k_i}{r} \left(\frac{\partial r}{\partial k_i} \right)_{k_{j \neq i}, K_i}, \tag{3.33}$$

where i is each step in the reaction mechanism. K_i indicates that the equilibrium constant is conserved and the thermodynamics of the reaction is not altered. This is quite a

powerful tool that will tell which steps contribute positively to the total rate, and which steps contribute negatively to the total rate.

3.7 Temperature programmed desorption (TPD)

A common way to experimentally study molecules interaction with a catalyst surface is temperature programmed desorption (TPD), something that was first introduced by Langmuir in 1916 [2, 133]. In a TPD experiment, a sample is prepared and pre-adsorbed with a probe molecule, for instance methanol. The sample is then slowly heated and what leaves the catalyst surface is measured as a function of temperature. The temperature at which the desorption peaks reveals the binding strength of the molecule to its binding site. The shape of the peak depends on the reaction order of the desorption mechanism [134].

A simple model to simulate TPD curves from first-principle calculations can be obtained by considering adsorption and desorption of a molecule on isolated and independent sites. With an adsorbed molecule A* and the empty site * we can perform the following derivation [135, 136]. Consider

$$
\mathrm{A^*} \underset{k_\mathrm{d}}{\overset{k_\mathrm{a}}{\rightleftharpoons}} * + \mathrm{A(g)}, \tag{3.34}
$$

where A(g) is the gas phase molecule. k_a is the rate constant for adsorption and k_d is the rate constant for desorption. In the mean-field assumption, the change of coverage of A, θ, is

$$
\frac{\mathrm{d}\theta}{\mathrm{d}t} = k_\mathrm{a} \frac{p}{p_\mathrm{ref}} (1 - \theta) - k_\mathrm{d}\theta \tag{3.35}
$$

where p is the gas-phase pressure of A and p_ref is a reference pressure. Using the ideal gas law, the concentration of A can be expressed as, assuming that the adsorption/desorption process equilibrates quicker than the heating rate and $\mathrm{d}\theta/\mathrm{d}t \approx 0$,[8]

$$
C = \frac{N}{V} = \frac{p}{k_\mathrm{B}T} = \frac{\theta}{1 - \theta} \frac{p_\mathrm{ref}}{k_\mathrm{B}T} \frac{k_\mathrm{d}}{k_\mathrm{a}} \tag{3.36}
$$

where $K = k_\mathrm{d}/k_\mathrm{a} = \exp\left(-\Delta G/(k_\mathrm{B}T)\right)$ is the equilibrium constant. At the same time, the mass balance in the flowing gas is

$$
FC = -A_0 W \frac{\mathrm{d}\theta}{\mathrm{d}t} = -\beta A_0 W \frac{\mathrm{d}\theta}{\mathrm{d}T} \tag{3.37}
$$

where F is the flow rate of the carrying gas, A_0 the concentration of the adsorption sites, W the sample weight, and $\beta = \mathrm{d}T/\mathrm{d}t$ the heating rate. Using these two expressions for the concentration (3.36) and (3.37), we obtain the following relation:

$$
\frac{-\beta A_0 W}{F} \frac{\mathrm{d}\theta}{\mathrm{d}T} = \frac{\theta}{1 - \theta} \frac{p_\mathrm{ref}}{k_\mathrm{B}T} \exp\left(\frac{-\Delta G}{k_\mathrm{B}T}\right) \tag{3.38}
$$

---

[8]One could be a bit more strict and set this to a small number $\mathrm{d}\theta/\mathrm{d}t = -\epsilon$, keeping this term and continue the derivation. This would give an extra term in equation (3.38), but since it will be negligible in comparison to the other terms we will neglect it here.

where ΔG is calculated from first-principles. Equation 3.38, is iterativly solved using

$$\theta_{i+1} = \theta_i + \left(\frac{\mathrm{d}\theta}{\mathrm{d}T}\right)\Delta T \qquad (3.39)$$

which, assuming a full initial coverage for each independent site, results in theoretical TPD profiles. This is a very simple way of modelling TPD spectra. It is not valid at high temperatures where the adsorb species will decompose since it allows for no reactions other than desorption to happen.

Chapter 4

Partial methane oxidation

" Ironically, the direct conversion of methane to derivatives, e.g., methanol, is thermodynamically feasible, but kinetically difficult."

– Pei Tang *et al.* [137]

Methane is not the most energetically favourable configuration of carbon and hydrogen, as can be seen in figure 4.1. With access to oxygen, the most favourable configuration is to completely oxidize methane into carbon dioxide and water. So, how can methane be only partially oxidized into something more useful than carbon dioxide? It would require a catalyst that controls the reactions and steer the selectivity towards, for instance, methanol. This chapter will discuss some of the catalysts we know can do this and how the work reported in this thesis aims to understand and potentially improve the selectivity of methane oxidation.

Partial oxidation of methane with oxygen from the air would be a dream reaction [138]

$$\frac{1}{2}O_2 + CH_4 \rightarrow CH_3OH. \tag{4.1}$$

In the same spirit, the ultimate goal is also to do this reaction at *ambient conditions*, *i.e.* atmospheric pressure and room temperature. Present methanol synthesis is far from fulfilling these conditions. Currently, industrial conversion of methane into methanol and other chemicals is done in a two-step process, where methane (or to be more accurate, natural gas) is transformed into synthesis gas, or syngas (CO and H_2) [24], which can then be used to create a wide spectrum of hydrocarbons or alcohols [139, 140]. This is typically done at very high temperatures and pressures, often up to $1000\,°C$ and pressures up to $30\,bar$ [141]. It also occurs at very large, centralized plants, since small plants are economically unfeasible [141, 142]. This is not in line with the very dispersed methane reserves in the world, for instance at remote oil rigs. An energetically cheaper and direct conversion of methane to methanol in one step would be a considerably more efficient route. However, this reaction is associated with intriguing challenges and has not yet been industrialized [20, 140].

4.1   What is needed for partial methane oxidation?

In some way, everything begins with the reactants on the left-hand side in equation (4.1). The first problem is to activate the oxygen, to split the stable oxygen molecule. This is certainly a requirement for a successful reaction, but not an easy one. To eliminate this particular problem, another oxygen source can be used. In some cases, laughing gas
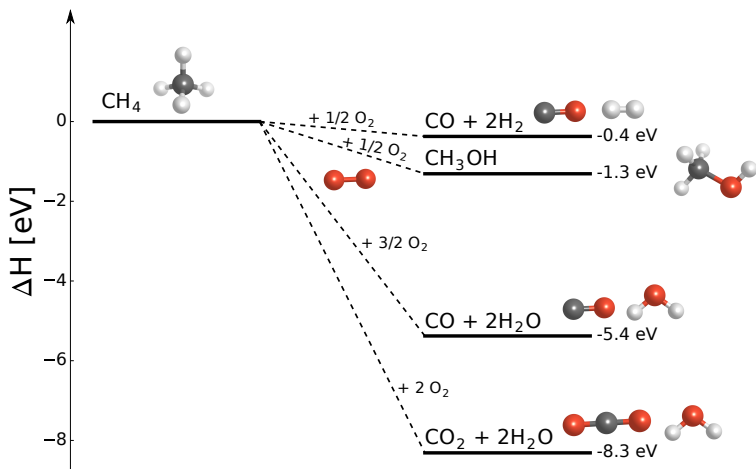
Figure 4.1: Diagram of different reaction enthalpies starting from methane and adding (different amounts of) oxygen. The experimental values are retrieved from [137, 140, 143].

(N_2O) [144] or even water [145] is used. From a sustainability point of view it would, however, be better to use air and O_2 as an oxidant.

The second issue is methane activation, breaking the first C-H bond on the CH_4 molecule. This is tricky because methane is a very stable molecule, has the strongest C-H bond of all hydrocarbons [137], a high free energy barrier at normal conditions[1], and is highly symmetric with no obvious attack point. Therefore a catalyst able to activate the methane is needed. It is generally not that difficult to find a catalyst that can do this, for instance with a palladium catalyst [146–149]. The main issue is rather the problem of selectivity.

Moving to the product side of the reaction in equation (4.1), how can we make sure that we get methanol and not something else? Controlling the selectivity of the reaction and steering it towards methanol, or any other product that is not CO or CO_2, is difficult. This is because thermodynamically it is much more favourable to form CO_2 and H_2O, as we have already seen in figure 4.1. "Over-oxidizing" methane into CO and CO_2 is therefore a likely outcome. One strategy to avoid over-oxidation could be to limit the amount of oxygen in the reaction, or the reactant's contact time with the oxidant [150]. However, the main problem is that once the first C-H bond is broken, breaking all the others is easier and all hydrogen atoms tend to be stripped off, ending up with CO or CO_2. On an ordinary extended surface or nanoparticle with large facets, this is possible since there are many neighbouring sites where the other hydrogen atoms can end up. To prevent this, isolated single-sites with a long distance to the next active site are needed. Single-site catalysis seem to be a requirement for partial oxidation of methane. These catalytically active single-sites may consist of one or more atoms [151]. Often these atom(s) are found on some kind of support, which keeps them isolated from each other,

---

[1]Low enthalpic barriers are not uncommon on many catalyst, but the entropic barrier at elevated temperatures is significant.
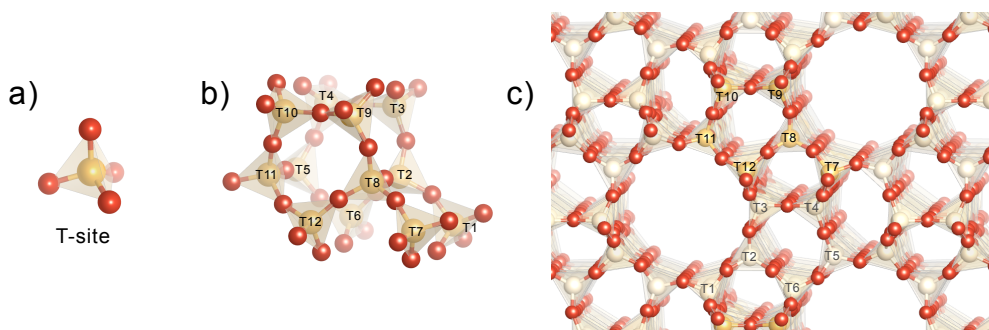
Figure 4.2: Zeolites are built from a) tetrahedras (T-sites) into b) secondary building units, SBU, which can then be combined into c) the full periodic structure. Here the MFI framework is used as an example with the numbering of the T-sites according to Olson et al. [156]

and keeps them from sintering into larger particles.

The partial oxidation of methane into methanol may seem impossible based on the previously mentioned problems. There are, nevertheless, systems in nature that actually can convert methane to methanol. The main example being the natural enzymes methane monooxygenases (MMO) [152–155]. The exact nature of the active sites in MMO is still a topic of discussion. There seems to be some consensus that in the different MMOs, di-metallic centres of iron or copper are involved. A less controversial feature of the MMOs is that they have a porous structure. This is believed to be important for selectivity. With a restricted pore size, large molecules and reactants can not enter and get to the active site, and large products cannot be created. Although MMO can convert methane to methanol there are some shortcomings, *e.g.* a very low production rate. For an industrially efficient implementation this is a serious shortcoming. It can also be difficult to separate the products using this homogeneous catalytic reaction, since these enzymes exist in solution. With a heterogeneous catalytic system that could convert methane to methanol, separating the liquid methanol, as compared to other gases, would be much easier and thereby more desirable.

4.2 Zeolites

Zeolites are a class of materials that are readily used in industrial catalysis [157]. Within partial methane oxidation, they are sometimes viewed as inorganic analogues to the methane monooxygenase (MMO) enzyme and similarly have pores and (often) metal ion sites. Zeolites ion-exchanged with certain ions, *e.g.* Cu, Ni, Co, and Fe, have been shown to be able to convert methane to methanol at ambient conditions [158–164].

Zeolites consists of corner-sharing SiO_4 and AlO_4 tetrahedrons, often called T-sites (see figure 4.2). These materials are generally thermodynamically meta-stable and template molecules are used in the synthesis. Around these template molecules the silicon oxide can
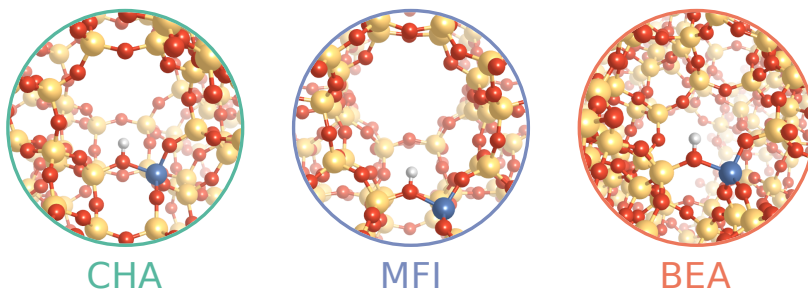
Figure 4.3: The structure of the Brønsted acid site in the CHA, MFI, and BEA zeolite framework.

be grown in various ways, depending on what template is used, creating pores and cages of different sizes. Some examples are Mordenite (MOR), zeolite beta (BEA), Chabasite (CHA), and MFI [157, 165]. ZSM-5 is an example of the latter and is, which we will come back to, especially interesting when it comes to partial methane oxidation.

By replacing Si^{4+} with Al^{3+}, a net charge is created which is compensated by a counter ion. When synthesized, the counter ions are usually Na^+, a proton, H^+, or ammonia [166]. In a later stage, these can be ion-exchanged with different cations to a metal ion, like Cu, Fe, Co, or Ni, creating sites often more active for redox reactions like methane oxidation. Given a Si:Al ratio, there exists a distribution of Al T-sites [167]. How these counter ions are arranged depends to some extent on the aluminium distribution. Two Al atoms can not be neighbouring T-sites and share the same oxygen, which is known as Löwenstein's rule [168, 169]. Other than this rule, we know that the distribution of Al and the number of Al pairs can be controlled to some degree depending on the synthesis method [170, 171]. The number of Al pairs can be important, since depending on the number of Al T-sites per cation, the oxidation state of the metal ion can vary.

With a proton as the counter ion, the site is known as a Brønsted acid site, figure 4.3 illustrates examples of these in a few different zeolite frameworks. Zeolites with only these acidic sites are widely used for processes such as cracking, isomerization and alkylation of hydrocarbons, which is for instance used in the oil and petrochemical industries [41, 172–174]. Water interacts quite strongly with these Brønsted acid sites [175], and the Brønsted acid sites are the main active sites for further reaction of methanol, into for instance DME (which is included in the following sections).

4.2.1 Zeolites for partial methane oxidation

Zeolites can be used to convert methane to methanol. Zeolites exchanged with copper ions are especially interesting. One of the most studied systems for heterogeneous direct conversion of methane to methanol is copper-exchanged ZSM-5 [158, 163, 166, 176–184]. The first successful experimental observation of methane-to-methanol conversion at ambient conditions, atmospheric pressure and a temperature of 448 K, required O_2 activation at much higher temperature (723 K) and the methanol had to be extracted in a third stage with a water/acetonitrile mixture [158]. One reason for the need of an
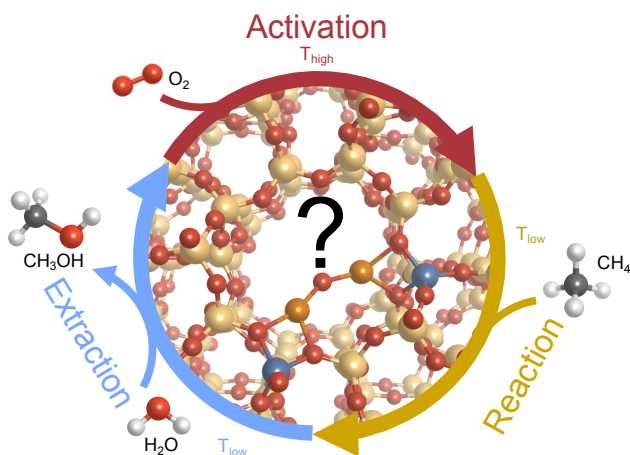
Figure 4.4: An illustration of the three-step reaction cycle of methane to methanol in zeolites: activation, reaction, extraction. What active site or sites this occurs on remains a big question.

extraction solvent, is that water reduces the methanol desorption barrier, as suggested by recent calculations [185]. Another hypothesis is that methoxy (CH_3O) species are formed, which would require a hydrogen or proton to desorb. These three steps, activation, reaction, and extraction, at different temperatures make the process unattractive for industrial application. A continuous catalytic cycle has been demonstrated [44, 45], but an efficient methane-to-methanol conversion has still not been obtained. Avoiding the over-oxidation of methane could be easier in the three-step cycle than in the closed cycle [150, 164], since the exposure to the oxidant is limited, *i.e.* the carbon never have direct access to the oxidant, but only to the oxygen in the prepared zeolite after the activation step. This would then suggest a higher selectivity towards methanol with the three-step process, but with a lower overall efficiency. An anaerobic oxidation mechanism of methane with water has also been proposed [145, 186]. There are some evidence that this could happen, although why methane would selectively dissociate over the Cu, rather than the reactive α-oxygen remains unanswered. By understanding how the Cu-ZSM-5 system works, the hope is that we will be able to design an even better catalyst. However, first we need to understand the three steps during the reaction: the oxygen *activation*, the *reaction* of methane, and the methanol *extraction*, as illustrated in figure 4.4. These can be seen as the three fundamental issues in partial methane oxidation, as already discussed in section 4.1: activating the oxygen, activating the methane, and selectively steer the reaction to the desired product. Moreover, we need to know which active sites are involved in the reaction.
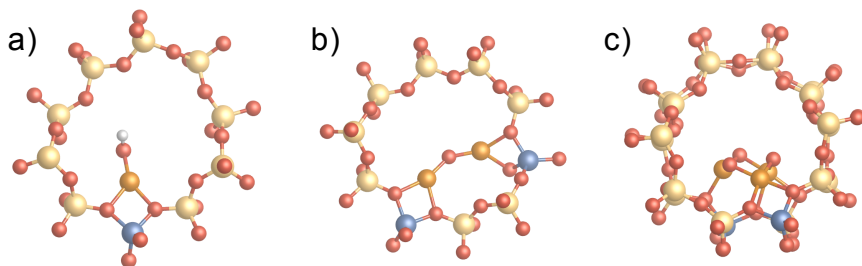
Figure 4.5: Three candidates for active sites: a) $[CuOH]^+$ b) $[Cu\text{-}O\text{-}Cu]^{2+}$ c) $[Cu_3O_3]^{2+}$. The structure in c) is adapted from [176].

4.2.2 The mystery of the active site

There have been many attempts to determine the active sites in metal ion exchanged zeolites [44, 158, 160, 166, 176–178, 180, 182, 185, 187–202]. For Cu-exchanged zeolites, the common oxidation states for Cu are 1+ and 2+ [203], indicating that one Cu cation can in principle compensate the charge of one or two Al T-sites [204]. Since we know that the Al distribution can vary, this complicates things. If there are pairs of Al T-sites, will there be one or two Cu ions associated with that site?
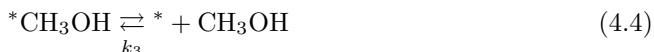
One possible candidate that has been proposed for Cu-exchanged zeolites is a $[Cu\text{-}O\text{-}Cu]^{2+}$ motif (which is the site illustrated in figure 4.4). This motif was experimentally identified with a characteristic spectroscopic signature in the UV-vis region around $22\,700\,cm^{-1}$. The appearance of this signature for zeolites with different Cu:Al ratio correlated with the methanol production [158]. This signature was later assigned to a bent $[Cu\text{-}O\text{-}Cu]^{2+}$ structure [181]. Since the $[Cu\text{-}O\text{-}Cu]^{2+}$ motif was identified, it has been extensively characterized, both experimentally and theoretically [144, 181, 184]. The $[Cu\text{-}O\text{-}Cu]^{2+}$ motif is a good candidate for active site, however the absolute need for this motif for methane-to-methanol conversion is not conclusive. For instance, Narsimhan *et al.* [44] were recently able to experimentally demonstrate a continuous catalytic methane-to-methanol cycle in Cu-ZSM-5 without the appearance of the UV-vis signature around $22\,700\,cm^{-1}$. Also, in recent theoretical studies [176, 205], trinuclear Cu-clusters were suggested as possible active sites in Cu-Mordenite and Cu-ZSM-5, while Kulkarni *et al.* [206] suggest a Cu monomer site in addition to the $[Cu\text{-}O\text{-}Cu]^{2+}$ and Cu_3O_3 motifs. Larger copper clusters have also been proposed as active species, especially at lower temperatures ($\sim 200\,°C$) [141, 164, 179, 207]. Clusters of up to nine copper ions have been studies theoretically, and could very well be possible active sites [207, 208]. Experimentally, X-ray Absorption Spectroscopy (XAS), and especially Extended X-Ray Absorption Fine Structure (EXAFS) can determine the coordination of atoms in a sample. For Cu-exchanged zeolites, there are experimental indications that there are CuO clusters or particles present in the system [179, 198]. However, since this is an averaging technique, it is impossible to know how many larger clusters compared to small clusters or isolated ions there are. Neither is it possible to know how active the different species are.

4.3 Metal dimer sites in ZSM-5 (Paper I)

The [Cu-O-Cu]$^{2+}$ motif is still a viable candidate for an active site, but perhaps not the only one. In a study by Tsai *et al.* [144], the different possible configurations of a [Cu-O-Cu]$^{2+}$ motif in the ZSM-5 zeolite were investigated. They found that there is a clear energetically favourable configuration at the crossing between the straight and sinusoidal channels in the framework. It should be noted, that not only Cu has been used for methane-to-methanol conversion in zeolites, but also Ni, Co, and Fe have been shown to have activity towards methanol [159, 160, 191]. An equally clear candidate for active site in these systems has, however, not been identified.

In **Paper I**, we study the [Cu-O-Cu]$^{2+}$ motif, for Cu and other transition metals by means of DFT and micro-kinetic modelling. Based on the model by Tsai *et al.* [144], we constructed a cluster model of the active site, *i.e.* we cut out a piece from the periodic structure around the active site and saturated the dangling bonds with hydrogens. The first question we addressed was how much of the surrounding zeolite structure we need to include in the cluster model to accurately describe the true periodic system. With different sizes of the cluster model we compared the adsorption energies of oxygen and methanol on the dimer motif, compared to the periodic structure (see Fig. 1 in **Paper I**). The results show that including the whole ring structure of the pore around the active site is important. It is also clear that using this *ring model* is a good compromise between accuracy in energy and computational cost.

Once we decided for the ring model, we considered a simple and direct reaction mechanism, namely

$$^*O + CH_4 \underset{k_1}{\rightleftarrows} {}^*OH, CH_3 \tag{4.2}$$

$$^*OH, CH_3 \underset{k_2}{\rightleftarrows} {}^*CH_3OH \tag{4.3}$$

$$^*CH_3OH \underset{k_3}{\rightleftarrows} {}^* + CH_3OH \tag{4.4}$$

where the first step is dissociative adsorption of methane with the formation of adsorbed -OH and -CH$_3$ groups on the metal dimer motif. The second step is the subsequent recombination of these groups into adsorbed methanol (*CH$_3$OH), and the third step is methanol desorption. We study two cases, a steady state case which includes methanol back-adsorption, and one transient model which does not, *i.e.* setting $k_3^- = 0$. This would correspond to the case when methanol is continuously and rapidly extracted from the reaction. Here we have assumed a mean-field distribution of adsorbed species and used ideal-gas expressions for the free molecules. Another restriction is that we do not consider oxygen activation, since it is not fully understood. One possibility is the formation of a peroxo intermediate (Cu-O-O-Cu) [183] followed by subsequent removal of the first and then the second oxygen atom. This possibility is similar to the proposed mechanism in ammonia selective catalytic reaction (SCR) in Cu-CHA [209], although in ammonia SCR the copper ions are believed to be mobile and connected to two NH$_3$ ligands, which is also supported experimentally [210, 211]. How mobile the Cu ions are during methane oxidation needs to be determined and will affect the understanding of this complicated reaction.
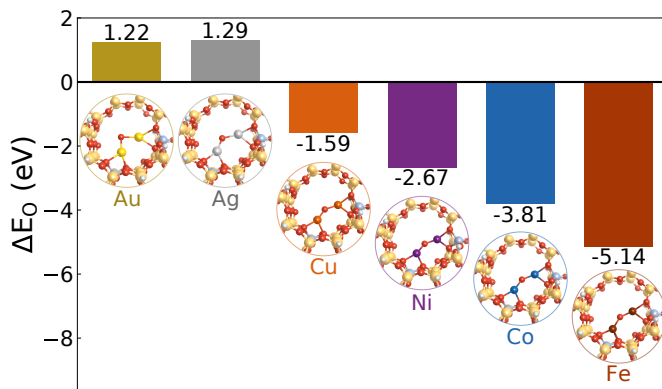
Figure 4.6: Oxygen adsorption energies for the dimer motif with Au, Ag, Cu, Ni, Co, and Fe, calculated with half an oxygen molecule as a reference.

The energies of intermediates and transition states for the $[\text{Cu-O-Cu}]^{2+}$ motif was calculated for Cu, Ni, Co, and Fe (see figure 2 in **Paper I**). Comparing oxygen adsorption energies shows that Ag and Au are unwilling to oxidize and form the α-oxygen in the first place, and are therfore unlikely candidates, see figure 4.6. As can be seen in the energy landscapes, we considered two methane dissociation barriers for Cu: the geometrically shortest reaction path through what resembles a surface-stabilized transition state with a -CH$_3$-group bound to one of the copper ions, and another path through a CH$_3$ radical-like transition state. Recently Latimer *et al.* [212, 213] have described these two different methane activation pathways, finding different scaling relations and arguably different physics for different classes of catalysts. Using the climbing image NEB method, we did not find the radical barrier. When using the alternative LSTQST method, as applied in the DMol^3 software, we did find a radical-like transition state for Cu. Although this barrier is $0.39\,\text{eV}$ lower than the surface-stabilized, the sensitivity analysis (see figure 4.8) reveals that it is only for Cu the first barrier is rate-determining, while the Ni, Co, and Fe systems remain unaffected by changes in the methane dissociation barrier. It also shows that considering the surface-stabilized or the radical barrier does not make a difference for the trend in elements. Another question that naturally arises, is whether the radical-like mechanism keeps its selectivity towards methanol or if it rather goes down a different pathway forming something else, for instance DME. Especially considering its radical nature it would seem possible that it reacts with something else – perhaps even with the zeolite framework wall.

The micro-kinetic results for experimental conditions of $1\,\text{mbar}$ and $523\,\text{K}$ are shown in figure 4.7. This shows a clear trend in catalytic performance (here measured using the half-time $\tau_{1/2}$, *i.e.* when half of the methane has been converted) between the different dimer sites. The time scale is reasonable for Cu, $2.2 \cdot 10^4\,\text{s} \approx 6\,\text{hours}$ (or $0.6\,\text{s}$ for the radical-like TS) , while unrealistically long for the others: $1.5 \cdot 10^9\,\text{s}$ for Ni, $3.0 \cdot 10^{19}\,\text{s}$ for Co, and Fe show no activity even at these extreme time scales. To put this into perspective; the Big-bang theory puts the age of the universe at 13.8 billion years or
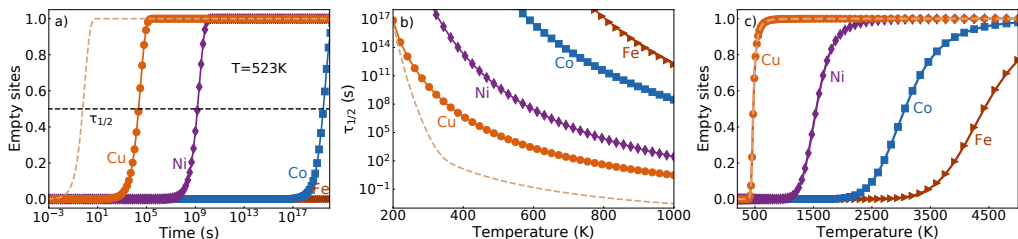
Figure 4.7: a) Coverage of empty sites, or methanol produced, for the Cu, Ni, Co and Fe dimer sites as a function of time at $523\,\mathrm{K}$. b) The reaction time $\tau_{1/2}$ as a function of temperature. c) Steady-state coverages of empty sites for the Cu, Ni, Co and Fe dimer sites as a function of temperature. The dashed lines for Cu are for the radical-like methane dissociation barrier.

$4.4 \cdot 10^{17}\,\mathrm{s}$ [214, 215]. The steady state kinetics with a methanol pressure of $10^{-6}\,\mathrm{bar}$ is shown in figure 4.7. Here we see that the $[\mathrm{Cu\text{-}O\text{-}Cu}]^{2+}$ site converts methane to methanol around $500\,\mathrm{K}$, while Ni, Co, and Fe require unrealistically high temperatures. They are unrealistic since they are high and since the ZSM-5 framework actually breaks around $1400\,\mathrm{K}$ [216]. There exists experimental evidence for methane-to-methanol conversion for Ni-, Co- and Fe-ZSM-5 zeolites [159–161]. This means that the model we propose here cannot be the full story. We propose two possible reasons why our model does not capture this; either that for Ni, Co and Fe the proposed reaction mechanism does not capture the essence of the reaction, or that this dimer motif is not a relevant active site for these elements.

To evaluate which step is important, we changed the energy of each step by $\pm 0.25\,\mathrm{eV}$ for Cu, Ni, Co, and Fe, and evaluated the changes in the kinetic behaviour (see figure 4.1). This demonstrates that the conclusion – that Cu is the best, followed by Ni, Co, and Fe – is robust and would not change by using a different energy description, *e.g.* including van der Waals interactions. An energy change of $\pm 0.25\,\mathrm{eV}$ is of the same order of magnitude as the shift in adsorption energies in zeolites when including van der Waals interaction [217]. The sensitivity analysis also shows that the methane dissociation barrier (TS1) is important only for Cu, while TS2 is important for Ni and Co, and desorption from the methanol state is important for Fe. The energy of the oxygenated site *O + CH4 is important for all considered metals. This analysis confirms that the trend in elements, Cu followed by Ni, Co, and then Fe, is robust and that the surface-stabilized or radical-like methane dissociation barrier does not change this conclusion. Similar trends when varying the transition metal cation in the $[\mathrm{M\text{-}O\text{-}M}]^{2+}$ motif have been obtained for different zeolite frameworks [164].

The oxygen adsorption energy does seem to capture this clear trend along the periodic table (Cu, Ni, Co, Fe): -1.59 eV for Cu, -2.67 eV for Ni, -3.81 eV for Co, -5.14 eV for Fe, -1.29 eV for Ag, and -1.22 eV for Au (figure 4.6). Co and Fe clearly bind the oxygen too strongly, making it difficult for the reaction to continue. The high tendency to bind oxygen for Co and Fe, may suggest that for these metals, the preferred active site structure is a more oxidized one with more than just one oxygen.

39
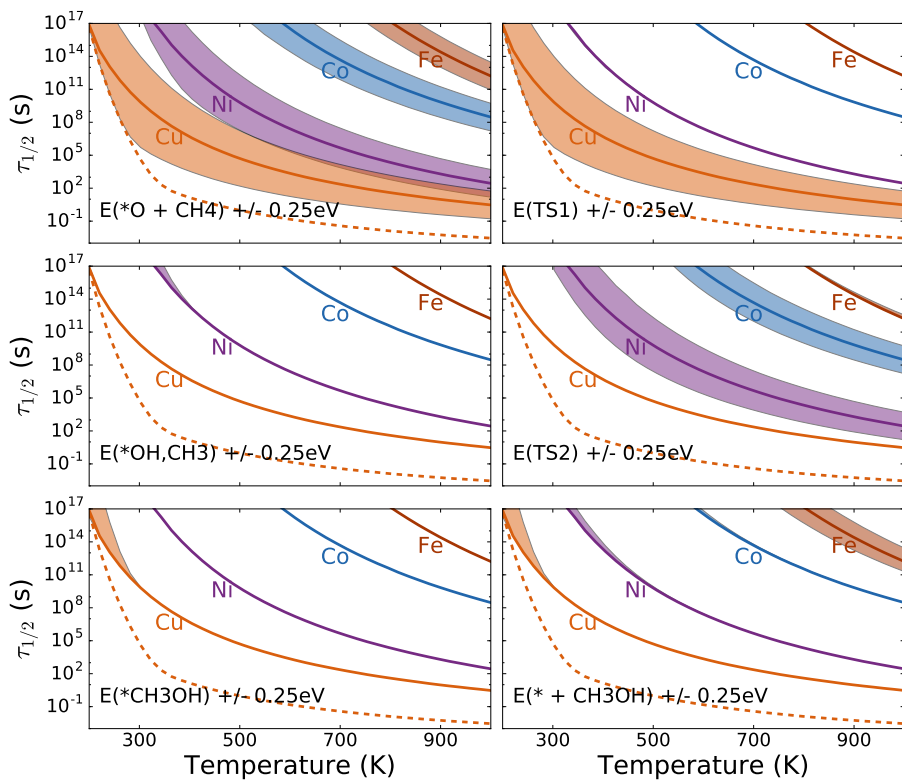
Figure 4.8: Change in $\tau_{1/2}$ when changing the energy of each intermediate by $\pm 0.25\,\mathrm{eV}$. From **Paper I**.
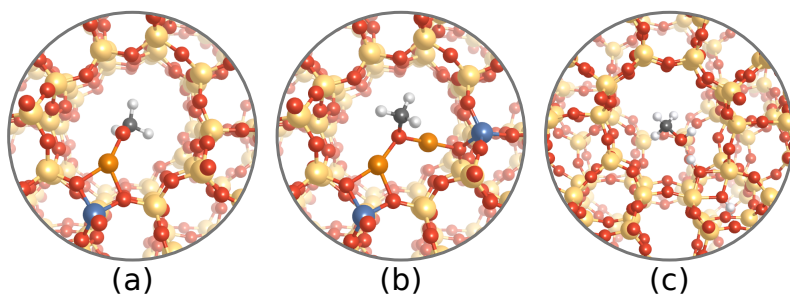
Figure 4.9: Methoxy bound to a) a copper monomer, b) a dimer, and c) methanol adsorbed on the silanol site.

4.4 IR spectroscopy and methanol TPD (Paper II and Paper III)

In **Paper II** and **Paper III**, the methanol interaction with zeolites, with and without copper, is investigated experimentally combined with first-principles calculations by means of infrared (IR) vibrational spectroscopy and methanol temperature programmed desorption (TPD). Comparing the experimental spectra at different temperatures for Cu-exchanged ZSM-5 and bare ZSM-5, it is clear that the Cu species are responsible for most of the interaction with methanol. One main conclusion from the experiments is that CO and formate, CHOO, peaks are only observed for the Cu-exchanged zeolite, indicating that the Cu-species are responsible for the further oxidation of methanol to CO and formate. The calculations confirm, together with other experimental literature that these peaks are indeed CO and CHOO on a copper monomer site, see Table 1 in **Paper II**. Frequencies were calculated for adsorbates on the $[Cu-O-Cu]^{2+}$ motif, a Cu monomer, a Brønsted acid site (Al + H$^+$). One interesting feature of the calculated frequencies is the shift in one of the C-H stretching modes for methoxy (OCH$_3$) adsorbed on the Cu monomer site (figure 4.9). Compared to methoxy on the dimer motif, one of the three C-H stretching modes has a low frequency at $2690 \, \text{cm}^{-1}$, compared to the others around $2900\text{-}3000 \, \text{cm}^{-1}$.

Another interesting conclusion from these studies, is the silanol model we came up with. We created OH-terminated silicon groups by splitting a water molecule over a Si-O-Si bond creating two OH groups as illustrated in figure 4.9c). The OH stretch frequency on this silanol site was calculated to $3760 \, \text{cm}^{-1}$, which compares to the experimental assignment of $3740 \, \text{cm}^{-1}$[218, 219]. Interestingly, this frequency shifts to $2790 \, \text{cm}^{-1}$ upon methanol adsorption to the silanol site, according to our calculations. This is around the experimentally seen band around $2780 \, \text{cm}^{-1}$. In **Paper II**, we assigned this peak to an the A, B, C triplet [220] which is associated with methanol interacting via hydrogen bonds with the Brønsted acid sites.

The methanol-TPD study in **Paper III** shows that at higher temperatures methanol is further oxidized to DME and CO (see figure 1 in **Paper III**). More DME is formed on

the samples without copper, indicating that it is the bare Brønsted acid sites that are the main active sites for methanol-to-DME conversion. The calculations show (see figure 3 in **Paper III**) that methanol binds stronger when coordinated to the Cu ions, while on the OH-coordinated sites, like the Brønsted acid site and the silanol group, methanol desorbs at lower temperatures.

From the TPD calculations, it is tempting to draw the conclusion that only the Cu-O(H)-Cu dimer is the relevant active site with copper, since the bare Cu monomer and dimer Cu-Cu bind too strongly and DME and CO has formed at high temperatures where these start to desorb methanol, and since the other CuOH binds too weakly. Although appealing, this might be a too bold conclusion to draw. We restricted our investigation to the bare sites (the Brønsted acid site and the silanol site), copper monomer, and copper dimer sites. There could very well be other site relevant for this reaction; copper trimers, tetramers, or even bigger clusters. Further, our TPD model is very simple and assumes independent and isolated sites with only methanol as possible adsorbant. We know from the experiment that DME and CO forms at higher temperatures, proving that the methanol species are not independent and that other products are formed.

4.5   Acidity and methanol-to-DME (Paper IV)

In **Paper IV**, we study one possible outcome from the extraction part of the methane-to-methanol catalytic cycle, namely the continued reaction of methanol to dimethyl ether (DME). This reaction usually takes place in hydrogen-exchanged zeolites over the Brønsted acid site (which we saw indications of in **Paper III**). The most commonly discussed reaction mechanism for methanol to DME conversion consists of two paths: the *associative* and the *dissociative* pathway [221, 222], which are illustrated in figure 1 in **Paper IV**. Both start with methanol adsorbing to the Brønsted acid site. In the associative mechanism, a second methanol reacts with the methyl group of the first methanol, forming DME and water. In the dissociative mechanism, the first adsorbed methanol is split into water and an adsorbed methyl group, sometimes called a *surface methoxy species* (SMS), considering the oxygen in the framework. Upon this methoxy species, a second methanol approaches and reacts to DME. All transition states involve an umbrella-like inversion of the methyl group [223], moving it from one species to the other. In figure 2 in **Paper IV**, we show the reaction landscape for the aluminium CHA zeolite, with and without MP2 corrections, and the turn-over frequency (TOF) for the associative and dissociative reaction paths with the MP2 corrections. The MP2-corrections are included in an attempt to improve the description of the energetics. From previous calculations [224] it is known that MP2-corrections address the underestimation of barriers by most non-hybrid density functionals. As can be seen in figure 2a in the paper, the pure DFT PBE-D3 results underestimate the transition state energies in the range of 0.15-0.30 eV. We see that at low temperatures the associative mechanism dominates, while at higher temperatures the dissociative mechanism has the higher TOF. This is also reflected in the degree of rate control analysis, where a shift in rate control from the associative barrier to the water methylation step (the first step in the dessociative mechanism) around the same temperature. At even higher temperatures the second
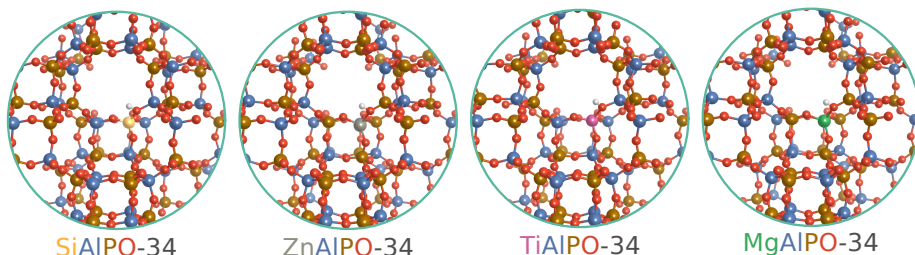
Figure 4.10: The Brønsted acid site in the different aluminophosphates zeotypes considered in **Paper IV**.

barrier, the methanol methylation step, becomes rate controlling.

The three transition states were found using the Automated Relaxed Potential Energy Surface Scans (ARPESS) package [121], with the breaking and forming of carbon bonds in the transferred methyl group as the reduced reaction coordinate. Once having a reaction mechansim and a routine for finding transition states, we exchanged the Al in the zeolite to B and Ga, which are in the same column as Al in the periodic table and have the same electron valence, and Fe, which can also be in a 3+ oxidation state. We did this for three zeolite frameworks, the CHA, MFI, and BEA, which were illustrated in figure 4.3. We also calculated the energy landscapes for the aluminophosphates SiAlPO-34, ZnAlPO-34, TiAlPO-34, and MgAlPO-34, which are illustrated in figure 4.10.

For all of these systems, we calculated two acidity descriptors, the shift of the O-H stretch frequency on the Brønsted acid site upon CO adsorption, *i.e.*

$$\Delta f_{\text{OH}} = f_{\text{OH}}[\text{Z-OH}] - f_{\text{OH}}[\text{Z-OH-CO}] \tag{4.5}$$

and the ammonia adsorption energy, *i.e.*

$$\Delta E_{\text{ammonia}} = E_{\text{Z-H-NH}_3} - (E_{\text{Z-H}} + E_{\text{NH}_3(\text{g})}). \tag{4.6}$$

We compare these in figure 4.11a) and see that for each framework they correlate linearly. In 4.11b-d) we show the energies of the three transition state and the methanol adsorption energy as a function of the shift of the O-H stretch frequency Δf_{OH}. It can be noted that the correlation coefficient R^2 is very high, which indicated a strong correlation, and the mean absolute error (MAE) is low.

Using the scaling relations of the OH shift acidity descriptor established in figure 4.11, we can evaluate the energy landscape for the reaction as a continuous function of acidity. Putting this into the microkinetic model, we obtain the solid lines in figure 4 in **Paper IV**. We clearly see that the MFI framework has a much higher turn-over frequency than BEA and CHA. We also see that the calculated TOF for the MFI systems (the purple points) are close to the solid line. Additionally, we can at these conditions, compare to experiments for H-ZSM-5 [225], which is the same as Al-MFI, represented by the black point in the figure 4 in **Paper IV**.

Furthermore, we compare the TOF from the full micro-kinetic model with a simplified model where we assume that the associative barrier is the rate-determining step, *i.e.*
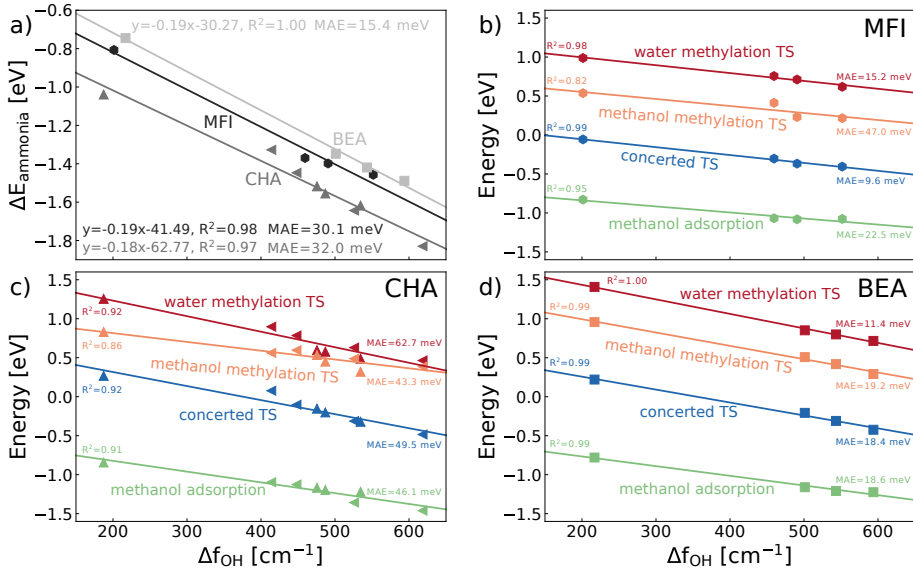
Figure 4.11: A comparison of a) the two acidity descriptors, and the linear correlation of the acidity and the transition state energies and the methanol adsorption energy for b) MFI, c) CHA, and d) BEA.

calculating the rate as

$$r_{\mathrm{model}} = \frac{k_B T}{h} \exp\left(-\frac{\Delta G_{\mathrm{ass}}}{k_B T}\right) \qquad (4.7)$$

where the free energy difference, ΔG_{ass} is the energy barrier from adsorbed methanol to the concerted transition state (the apparent associative barrier). The results are in fair agreement with the solid lines from the full micro-kinetic model. The difference can be explained by the fact that this model implicitly assumes that the full coverage of adsorbed methanol (Z-H-CH$_3$OH). From the steady-state coverages (which can be found in figure S3 in the supporting information to **Paper IV**) obtained from our micro-kinetic model we see that the coverage varies as a function of Δf_{OH}, explaining the deviations between the simple model and the full micro-kinetic results.

4.5.1 Geometric and electronic effects on acidity

As can be seen in figure 4.11, the results are framework dependent. The fact that the framework has an impact on acidity is not that strange when considering the structure of the Brønsted acid site [Al-O(H$^+$)-Si]. A simple way of looking at this is to consider the covalent nature of the Al-O, Si-O, and O-H bonds at the Brønsted acid site. The threefold coordination of the oxygen atom is similar to that of the H$_3$O$^+$ ion. What the framework then does, is to constrain the angles of the threefold coordinated oxygen, thus weakening the OH bond and increasing the acidity [226]. Having several aluminium sites close together can also affect the local structure of the threefold coordinated oxygen, thus
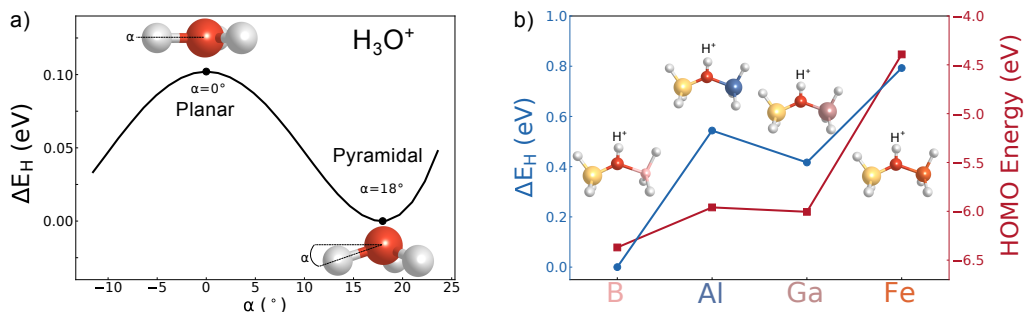
Figure 4.12: a) the geometrical effect on acidity illustrated by the angle dependence of the hydronium cation (H_3O^+), and b) the electronic effect illustrated by the relative hydrogen abstraction energy ΔE_H is obtained as the energy gained by binding the proton, which is also correlated to the HOMO level (red squares).

can high aluminium distribution also affect acidity. This geometric effect is illustrated in figure 4.12, where the relative hydrogen abstraction energy

$$E_H = E_{H_3O^+} - (E_{H^+} + E_{H_2O}), \tag{4.8}$$

is used as a measurement of acidity. This is simply the binding energy of the proton. In figure a), the geometric effect is illustrated by changing the angle of the H_3O^+ ion, as it goes from the preferred pyramidal shape (with $\alpha = 18°$, to the less stable two dimensional planar structure. In figure b), the electronic effect on the relative hydrogen abstraction energy is illustrated by taking the T-sites in the zeolite framework into account. This model was constructed by cutting out the Si and Al T-sites in the MFI framework and hydrogen terminating the dangling bonds. Only the proton was allowed to relax. The blue circles are the calculated acidity (ΔE_H) for B, Al, Ga, and Fe. This electronic effect is further illustrated with the highest occupied molecular orbital (HOMO) energy in red squares. The shift in the HOMO level explains the change in acidity quite well. The difference in energy scales should be noted here. The geometric effect in a) is clearly much smaller than the effect obtained when changing the electronic structure by changing the ion in b), which is also why the framework difference (the geometric effect) is relatively small compared to changing the exchange ion in **Paper IV**. The energies in figure 4.12 were calculated with the DMol[3] software, using the PBE functional.

4.6 Molybdenum sulfide clusters (Paper V and Paper VI)

Starting in **Paper V** and continuing in **Paper VI** we study partial methane oxidation on Mo_6S_8 clusters with sulfur, H_2S to be more precise, rather than oxygen as oxidant. This is an important reaction for cleaning sour natural gas from sulfur contaminants. Similarly to the ion sites in zeolites, this reaction also happens over isolated single sites on the clusters. Another reason to look into this is the possibility of running this reaction also in zeolites [227], which would be an interesting comparison to make in the future.
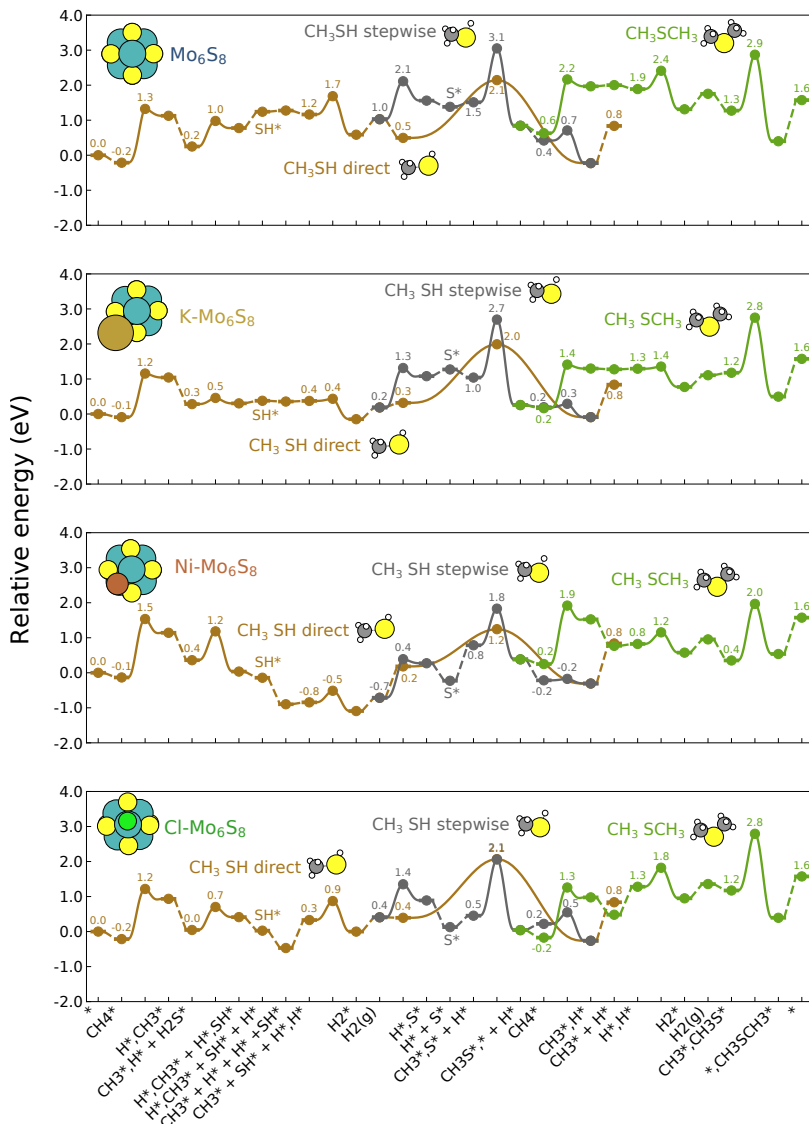
Figure 4.13: Energy landscapes for $CH_4 + H_2S$ to $CH_3SH + H_2$ via a direct pathway (brown) and a stepsize pathway (grey) and the longer pathway to dimethyl sulfide CH_3SCH_3 (green) on the bare Mo_6S_8 cluster, and the K-, Ni-, and Cl-promoted clusters.
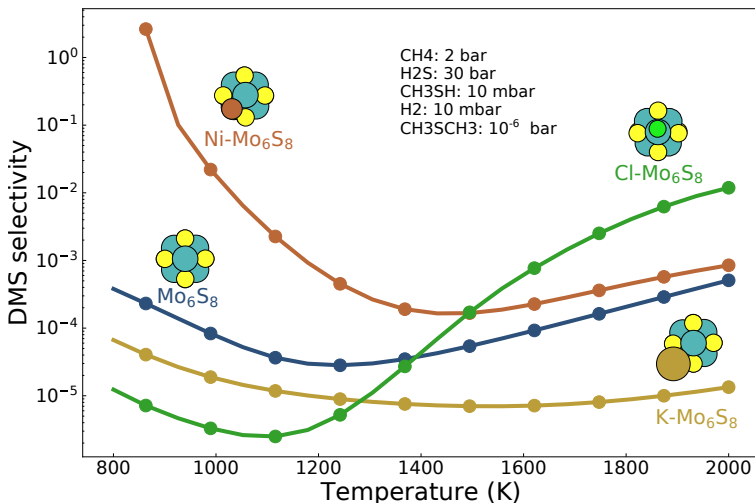
Figure 4.14: Selectivity, the ratio between the TOF for CH_3SCH_3 and CH_3SH from **Paper VI** for the four different clusters.

These two studies are based on promoting the Mo_6S_8 cluster with single atoms. We promote the cluster with one K atom or one Ni atom in **Paper V** and also with the more electronegative Cl in **Paper VI** . The energy landscapes for the reaction on the four different clusters can be seen in figure 4.13, where only the direct pathway was considered in **Paper V**, and all three in **Paper VI** (where we also considered the Cl-promoted cluster).

Paper V assumes a direct and simple reaction mechanism to the methanol analogue, methanethiol (CH_3SH). Here we use a double-site notaion [A*,B*], corresponding to an -S-Mo- site with A adsorbed to the sulfur and B on the molybdenum. The calculated turnover frequencies in **Paper V** clearly show that the promoted Mo_6S_8 clusters are far superior to the bare cluster. Which promotor is better changes with temperature. A degree of rate control analysis in the same paper shows that the rate-determining step for K-Mo_6S_8 at high temperature is the hydrogen formation, while for Ni-Mo_6S_8 the methane dissociation is controlling. At lower temperatures ($<900\,\mathrm{K}$) the Ni-promoted cluster becomes limited by the CH_3SH desorption, an effect that also is reflected in the TOF, where Ni enters a non-linear regime with prohibiting coverage effects.

In order to include more reaction pathways, and be able to look at selectivity, we expand our model in **Paper V**. We do this by including diffusion steps in a parametric way, *i.e.* setting all diffusion barriers to the same low value. This enables us to also consider the two paths to form CH_3SH, the direct via the CH_3* and SH* combination, and the stepwise via the CH_3S* and H* combination, as well as the pathway to form dimethyl sulfide (DMS) CH_3SCH_3.

Figure 4.14 shows the selectivity for CH_3SCH_3, compared to CH_3SH, as a function of temperature at industrially relevant pressures. We can conclude that with higher activity overall, as for the K-promoted cluster (see figure 3 in **Paper VI**), the selectivity is lower,

while for the Ni-promoted cluster, which has a lower activity overall, the selectivity is higher. This illustrates that it is difficult to ensure high activity and high selectivity at the same time.

4.7 Conclusions from the appended papers

The aim of this thesis has been to investigate partial oxidation of methane, primarily into methanol, using Cu-exchanged zeolites, and to understand the different aspects of direct methane-to-methanol conversion. This has been done by combining electronic structure calculations and microkinetic modelling, and comparing with experiments via IR spectroscopy and adsorption energies in the TPD profiles.

By comparing adsorption energies for different model sizes, we showed that it is important to include enough of the pore structure to accurately describe adsorbates on the $[Cu-O-Cu]^{2+}$ site in ZSM-5. The study of the metal dimer motif in **Paper I** also shows that the $[Cu-O-Cu]^{2+}$ is a relevant candidate for active site only in the case of Cu-ZSM-5. Furthermore, we showed that the methane dissociation barrier is only important for the Cu motif, and even though the two different barriers, one surface-stabilized and one radical-like, evaluated for Cu differ with almost $0.4\,eV$, the conclusion that the dimer motif is reasonable for Cu, but not realistic for Ni, Co, or Fe, did not change. It does, however, raise a question about which barrier is correct, especially since a climbing NEB algorithm did not find the radical-like barrier. This remains as a future challenge.

Entropy in zeolites is something that could be important and that could be modelled differently [228]. We used a simple ideal gas approximation, with the pressure measured or set outside the zeolite. This is a quite generous definition. It assumes that the molecule can move freely in a volume, defined by the pressure through the ideal gas law $pV = Nk_{B}T$. In a confined space, like in a zeolite, this volume is much smaller and restricted by the pore channel diameter in two directions – maybe it could be modelled as a one-dimensional ideal gas along the pores. At least in some way, the confinement will affect the entropy of the gas molecules [229].

The comparison between experimental and calculated IR frequencies in **Paper II** confirms that Cu species in Cu-ZSM-5 are responsible for the further oxidation of methanol to carbon monoxide and formate. Calculated frequencies for methoxy on a copper monomer give one C-H stretching mode close to a broad peak seen in experiments. This remains to further investigate.

In the continuing **Paper III**, we used a straightforward model to compute TPD profiles of methanol desorption from different adsorption sites. This we did for the CHA framework (SSZ-13) and the MFI framework (ZSM-5). One conclusion from this study is that the choice of T-site matters. In **Paper II** we studied one of the T-sites obtained from the $[Cu-O-Cu]^{2+}$ motif, which turns out to be a T7 site. On the bare Brønsted acid site, the OH stretch frequency was calculated to $3103\,cm^{-1}$, while the experimental assignment is around $3620\,cm^{-1}$. Later, in **Paper III**, we studied the T12 site (which is the most stable for methanol adsorption). The OH stretch frequency on this site was calculated to $3689\,cm^{-1}$, which agrees much better with the experimental assignment.

In the TPD simulations our model assumes that all sites are isolated and independent,

meaning that there is no interchange between different sites. It also assumes that methanol is pre-adsorbed and that methanol leaves, without the possibility of reacting to something else. From the experiments we know that the methanol will react to DME and CO at high temperatures, showing that there are limitations to our TPD model.

Paper IV broadens the investigation of partial methane oxidation to also look at other products than methanol, in this case DME. This happens mainly over the bare Brønsted acid site, where the acidic strength determines the activity. Here we show that there is a clear correlation between the acid strength and the methanol-to-DME activity, and that it is different for different frameworks, where the MFI framework is more active than the BEA and CHA frameworks. Preliminary results indicate that it matters which oxygen around the T12 site in MFI the reaction occurs on. This is something we will investigate more closely. However, the agreement with the experimental results and the calculated TOF of the site we modelled is promising. Our work on the acidity gives some hope as to how to possibly change the selectivity between the products in methane-to-methanol conversion. This is something our experimental colleagues are pursuing by trying to tune the acidity of the zeotype catalyst by changing the Al framework atoms to Fe or combining them [230].

Paper V demonstrates that partial oxidation of methane should also be possible on Mo_6S_8 clusters, but that promoting the clusters is necessary, here we tried Ni or K and found that both are more active than the bare cluster. The expanded reaction mechanism in **Paper VI** includes diffusion between the different clusters in a parametric way. This enables us to look at more reaction pathways and look at the selectivity between CH_3SH (methanethiol) and CH_3SCH_3 (DMS). Here we see that selectivity to DMS can be increased, but at the price of lowering the overall activity. It would also be interesting to see if methanol can be a product on these clusters with water as an oxidant. These two papers also offers some inspiration as to how it could be possible to expand the reaction mechanism in the zeolite systems. Although in the zeolites, it might be necessary to model a range of different sites, containing the exchange metal (copper), monomers and dimers, as well as the Brønsted acid sites which is important for the continued reaction to the dimethyl product (in zeolites DME).

Chapter 5

Reflections and conclusions

> "
> I suppose it is tempting, if the only tool you have is a hammer, to treat everything as if it were a nail."
>
> – Abraham Maslow [231]

Modelling zeolites and molybdenum sulfide clusters is not trivial. What active site to model is always tricky; what T-site(s), what aluminium distribution et cetera, is always something to contemplate over and (re-)consider. Oftentimes the best way to move forward is to not get stuck in these worries and simply *hammer away*, but then afterwards take a step back and reflect on what was assumed and what followed from that. In this chapter, I give some reflections on what we have concluded and the assumptions we have made and how we could move forward, and summarize what this work has contributed to the research field.

5.1 Reflections on the computational methods

There are many ways of modelling zeolites. In our first study we chose to use a cluster model approach, where we cut out a piece of the periodic structure and solve the electronic structure with a code that use local basis sets to represent the wavefunctions. In that case, the way the cluster was cut out matters. By evaluating a number of cluster sizes we finally decided on a ring model consisting of 40 T-sites, saturating the dangling bonds with hydrogens. Here we used the more or less standard DFT-PBE description. Often dispersive forces are believed to be important in zeolitic materials, due to the confined space. Here we are forgiven for omitting van der Waals interaction since we are looking at trends. This is confirmed in the sensitivity analysis which varies each energy significantly enough to capture any typical van der Waals interaction energy. Later we turned to using the complete unit cell with periodic boundary conditions. We also used the D3 correction to the PBE functional, which is a relatively cheap and easy way of including van der Waals interaction. It should be noted that we did not thoroughly or exhaustively explore the exchange-correlation functional dependence in any of our studies. It can be argued that the description of the correlation and the improvement of the self-interaction error needs to be carefully investigated and properly implemented in the computational scheme. Using a Hubbard approach to localize some electronic structure or moving to a costly hybrid functional are possible ways of doing so. How to accurately resolve the oxidation state of the copper ions, Cu^{1+} and Cu^{2+}, is a worry in zeolites. To describe this properly it could be necessary to better describe the self-interaction. When looking

at trends, however, as we often do, we are often forgiven the choice of xc-functional, and the trends remain resolute.

We have not looked into how large the self-image interaction is in our systems. It could be that the active site motif interacts with its own periodic image. Especially stress and strain induced by the defect that is the active site could be long range. It is experimentally known that the zeolite lattice expands when copper is exchanged into the zeolites [210]. Computational cost and the extent of the calculations needed, prevents us from a more thorough investigation of this effect. Other potentially important features, like the aluminium distribution and counter-ion coverage, are too large-scale to be treated with only DFT. Here it is possible to imagine going towards empirical potentials, trained with DFT results, or a cluster expansion approach, where the energy of structures are evaluted by expanding in terms of dimer, trimer, and higher order cluster interactions. This could potentially give results that are relevant on the macroscopic scale.

Other possibilities of modelling zeolites include the use of a multi-scale type of approach, where it is possible to use a higher level of theory for the active site and treat the rest of the framework on a lower level. Here there are two main fields. One is the cluster approach, where a piece of the structure is cut out and treated with a higher level of theory, usually post Hartree-Fock, and where the dangling bonds usually are saturated with hydrogen bonds [232–236]. The other approach is to use an embedded potential method, where there is a region within which a higher level of theory is used and without a lower level of theory. On the boundary between these two regions it is made sure that the potential from both methods match [237].

The micro-kinetic modelling in this work has been performed in the mean-field approximation. This is usually a good first approximation. It can, however, be discussed whether isolated sites in zeolites and whether isolated molybdenum sulfide clusters are accurately represented in the mean-field limit. The alternative, performing a kinetic Monte-Carlo simulation, would be an interesting study. The main issue here is to be able to describe all possible events that would need to be included in a kinetic Monte-Carlo study. Diffusion of different species between active sites or molybdenum sulfide clusters, adsorption of all possible species on the dual sites. There are, in the $[Cu-O-Cu]^{2+}$ motif three atoms – can three different species be adsorbed on the motif? Can any three adsorbates be adsorbed? All of these possibilities would need to be included (or with good reason excluded) from a kinetic Monte-Carlo simulation. This is quite cumbersome. Since these are small systems, each adsorbate would change the energy potentially quite differently, meaning that linear scaling relations could be difficult to obtain. Molecular dynamics or ab initio molecular dynamics simulation would be another approach which could potentially capture the vast complexity of the reactions. This is, however, also relatively expensive.

To summarize, the computational methods we have used in this work have been justified and good enough to address the questions we have asked. There is certainly room for improving the description of these systems, but the level of description should be chosen to be reasonable and accurate enough with regards to the questions. In this respect it is nice to realize that "trends are forgiving"[1].

---

[1]Anders Hellman, personal communication.

5.2 Reflections on the partial methane oxidation reaction

The methane-to-methanol reaction is a tricky reaction to study. The fundamental difficulty is the selectivity issue, as previously mentioned. To avoid the complete oxidation of methane and oxygen to carbon dioxide and water, it is necessary to control the reaction and make sure the selectivity to the partially oxidized species is higher. It does not really matter which partially oxidized products are obtained, as long as it is possible to control it to some degree and as long as it is a more useful product than CO_2. Methanol would be the simplest product, chemically speaking, but if the methanol is further converted into DME, that would still be desirable. One of the key features of zeolites is that it is believed that the methane oxidation takes place on isolated active sites, probably copper or iron sites. The fact that these sites are isolated is probably what stops the over-oxidation to CO_2. Which active site the reaction occurs on is still under debate. Experimental evidence for the structure of the active sites is difficult to obtain. The UV/vis peak around $22700 \, cm^{-1}$ assigned to the $[Cu-O-Cu]^{2+}$ motif does not seem to be necessary to observe methane-to-methanol conversion. EXAFS experiments can measure the average coordination number of different atoms. This could give an indication as to the preferred size of copper oxygen clusters, but it is only an averaging techniques, and might not capture the most active site. The fact that it is so difficult to experimentally determine the active sites makes it even more relevant to computationally model these systems, as it is cheaper and easier to perform computations rather than experiments.

It could very well be that the reaction happens on many different types of sites, or that different parts of the reaction happens on different sites. For instance, methane is probably oxidized to methanol or methoxy species on the copper sites, while DME is probably formed from methanol on the Brønsted acid sites. Another aspect is that, at least for some zeolitic reactions, like ammonia selective catalytic reaction in the chabazite zeolite, the active copper site is probably quite mobile [201, 209]. How this affects the reaction, if the different active sites change during the reaction, or if the active sites communicate with each other, is something that has not been investigated.

Since there are still many candidates for active site, the reaction mechanism is still not known. Recent studies have suggested that water can oxidize the Cu sites through a slightly different mechanism, where the methane is activated on the Cu rather than on the reactive α-oxygen in the $[Cu-O-Cu]^{2+}$ motif [145]. This is also supported experimentally [186]. Interestingly, the concentration of Brønsted acid sites have been linearly correlated with the concentration of methoxy species [145]. The proposed explanation for this is that methane splits over a copper complex and gives its proton to the framework oxygen next to the framework Al atoms, forming an acid site next to the copper complex [145].

Since there are both theoretical and experimental indications that there are even larger copper clusters in the zeolite, and that these very well may be active, what role does the zeolite play? Are they really necessary for the reaction? Is it possible to construct another catalyst that can support these clusters? Perhaps zeolites can be viewed as just that, a support that keep the copper clusters highly dispersed.

5.3 Contribution to the field

Finally, how has the work presented in this thesis contributed to the research field? Considering the three main parts of the partial methane oxidation (activation, reaction, extraction), we have contributed to two out of three; the reaction part and the extraction part.

Concerning the reaction part, we have investigated a very commonly assumed candidate for the active site, namely the $[\text{M-O-M}]^{2+}$ motif, and have likely excluded this motif for metal ions other than copper. This gives some insight into future studies on what the most relevant active sites could be in other zeolites. Furthermore, our experimental collaborations involving IR spectroscopy and TPD measurements has confirmed that copper is indeed necessary for methane-to-methanol conversion, and we have excluded the simplest copper monomer sites to be the main methanol adsorption site.

Our contribution to the understanding in the extraction part is mainly the acidity descriptor for methanol-to-DME and the insight that tuning the acidity, by replacing the Al with for instance B or Fe, provides a way of favouring the formation of methanol by prohibiting the formation of other products. This is something our experimental colleagues are pursuing [230].

The understanding of partial methane oxidation was also broadened to the partial methane sulphurization on molybdenum sulphide clusters. On this smaller system, we used micro-kinetic modelling to investigate the selectivity in a bigger reaction network. The conclusions from these studies will provide insight to the methane-to-methanol reaction in zeolites, as the reaction mechanisms are very similar.

Micro-kinetic modelling has been used throughout most of this work. There are, to my knowledge, very few, if any, existing studies where full micro-kinetic modelling has been attempted in zeolites for methane-to-methanol conversion. Although not without difficulties, this powerful tool can help to shed light on this complicated reaction.

Acknowledgements

The work presented in this thesis was carried out at the Division of Chemical Physics at the Department of Physics and the Competence Centre for Catalysis (KCK) at Chalmers University of Technology, Göteborg, Sweden, from July 2014 through April 2019.

I would also like to thank:

My main supervisor Anders Hellman, for everything. A constant source of inspiration and optimism. With your support and encouragement it always works out in the end.

My examiner and co-supervisor Henrik Grönbeck, for all the help, support, and for all discussions. And for letting me teach quantum mechanics.

Our experimental collaborators Per-Anders Carlsson and Xueting Wang. Thank you for all our discussions and for making experiments understandable.

Felix Studt, Phillip Plessow, and the rest of the IKFT group at Karlsruhe Institute of Technology. Thank you for a very nice research trip.

My officemates, past and present: Mikael, Unni, Maxime, Matthias, Stefan, Pooya, and Adriana. Thank you all for putting up with me and all my questions.

Everyone at Chemical Physics for creating a nice atmosphere. In particular everyone in the theory council: Chris, Maxime, Adriana, Mikael, Mikkel, Lin, Unni, Alvaro, Michael, Baochang, Matthias, Noemi and Lucy. Thank you for keeping the council the best council there is at Chemical Physics.

Igor for letting me ask tricky questions and for asking questions back.

Everyone I've had the privilege to teach with, and especially Jonathan for giving me so many nice opportunities.

Bibliography

[1] J. J. Berzelius. *Årsberättelse om framstegen i fysik och kemi.* p. 245. Stockholm: Royal Swedish Academy of Sciences, 1835.

[2] B. Lindström and L. J. Pettersson. A Brief History of Catalysis. *CATTECH* **7**.4 (2003), 130–138. DOI: `10.1023/A:1025001809516`.

[3] A. Libavius. *Alchemia.* Frankfurt: Johannes Sautrius, 1597.

[4] E. Fulhame. *An Essay on Combustion, with a View to a New Art of Dying and Painting. Wherein the Phlogistic and Antiphlogistic Hypotheses Are Proven Erroneous.* London: Printed for the author, by J. Cooper, 1794.

[5] J. Wisniak. The History of Catalysis. From the Beginning to Nobel Prizes. *Educación química* **21** (2010), 60–69.

[6] G. Ertl. *Gerhard Ertl - Nobel Lecture: Reactions at Surfaces: From Atoms to Complexity.* 2007. URL: `https://www.nobelprize.org/prizes/chemistry/2007/ertl/lecture/` (visited on 04/03/2019).

[7] L. J. Pettersson. *KTH — Jöns Jacob Berzelius - the Man Who Invented Catalysis?* `https://www.kth.se/en/che/archive/arkiv/berzelius-1.184145`. 2013. (Visited on 03/30/2017).

[8] P. Collins. The Pivotal Role of Platinum in the Discovery of Catalysis. *Platinum Metals Review* **30**.3 (1986), 141–146.

[9] H. Davy. Some New Experiments and Observations on the Combustion of Gaseous Mixtures, with an Account of a Method of Preserving a Continued Light in Mixtures of Inflammable Gases and Air without Flame. *Philosophical Transactions of the Royal Society of London* **107** (1817), 77–85.

[10] V. Smil. Detonator of the Population Explosion. *Nature* **400**.6743 (1999), 415–415.

[11] A. Hellman et al. "Ammonia Synthesis: State of the Bellwether Reaction". *Comprehensive Inorganic Chemistry II.* Elsevier, 2013, pp. 459–474. DOI: `10.1016/B978-0-08-097774-4.00725-7`.

[12] *Composition of Natural Gas.* `http://naturalgas.org/overview/background/`. 2013. (Visited on 09/30/2016).

[13] *BP Statistical Review of World Energy 2018.* `http://www.bp.com/statisticalreview`. (Visited on 04/15/2019).

[14] R. K. Pachauri, L. Mayer, and Intergovernmental Panel on Climate Change, eds. *IPPC, 2014: Climate Change 2014: Synthesis Report.* OCLC: 914851124. Geneva, Switzerland: Intergovernmental Panel on Climate Change, 2015, p. 87.

[15] D. T. Shindell et al. Improved Attribution of Climate Forcing to Emissions. *Science* **326**.5953 (2009), 716–718. DOI: `10.1126/science.1174760`.

[16] C. D. Elvidge et al. Methods for Global Survey of Natural Gas Flaring from Visible Infrared Imaging Radiometer Suite Data. *Energies* **9**.1 (2016), 14. DOI: `10.3390/en9010014`.

[17] J. Lelieveld and P. J. Crutzen. Indirect Chemical Effects of Methane on Climate Warming. *Nature* **355**.6358 (1992), 339.

[18] S. Pacala and R. Socolow. Stabilization Wedges: Solving the Climate Problem for the Next 50 Years with Current Technologies. *Science* **305**.5686 (2004), 968–972. DOI: 10.1126/science.1100103.

[19] A. Caballero and P. J. Pérez. Methane as Raw Material in Synthetic Chemistry: The Final Frontier. *Chemical Society Reviews* **42**.23 (2013), 8809–8820. DOI: 10.1039/C3CS60120J.

[20] A. I. Olivos-Suarez et al. Strategies for the Direct Catalytic Valorization of Methane Using Heterogeneous Catalysis: Challenges and Opportunities. *ACS Catalysis* **6**.5 (2016), 2965–2981. DOI: 10.1021/acscatal.6b00428.

[21] M. L. Jensen. SEGES Opsamler Metan i Mulehøjde. *SEGES Landbrug & Fødevarer* (2018). URL: https://www.landbrugsinfo.dk/miljoe/klima/sider/kn-18-seges-opsamler-metan-i-mulehojde.aspx.

[22] W. Taifan and J. Baltrusaitis. CH4 Conversion to Value Added Products: Potential, Limitations and Extensions of a Single Step Heterogeneous Catalysis. *Applied Catalysis B: Environmental* **198** (2016), 525–547. DOI: 10.1016/j.apcatb.2016.05.081.

[23] W. Taifan et al. CH$_4$ and H$_2$S Reforming to CH$_3$SH and H$_2$ Catalyzed by Metal-Promoted Mo$_6$S$_8$ Clusters: A First-Principles Micro-Kinetic Study. *Catalysis Science & Technology* **7**.16 (2017), 3546–3554. DOI: 10.1039/C7CY00857K.

[24] J. R. Rostrup-Nielsen. Production of Synthesis Gas. *Catalysis Today* **18**.4 (1993), 305–324. DOI: 10.1016/0920-5861(93)80059-A.

[25] *Wikimedia Commons Figure: Catalysis Scheme.* 2017. URL: https://commons.wikimedia.org/wiki/File:CatalysisScheme.png.

[26] *Wikimedia Commons Figure: Volcano plot.* 2017. URL: https://commons.wikimedia.org/wiki/File:Volcano_plot.png.

[27] J. Kašpar, P. Fornasiero, and N. Hickey. Automotive Catalytic Converters: Current Status and Some Perspectives. *Catalysis Today.* Fundamentals of Catalysis and Applications to Environmental Problems **77**.4 (2003), 419–449. DOI: 10.1016/S0920-5861(02)00384-X.

[28] S. Aiba, M. Shoda, and M. Nagatani. Kinetics of Product Inhibition in Alcohol Fermentation. *Biotechnology and Bioengineering* **10**.6 (1968), 845–864. DOI: 10.1002/bit.260100610.

[29] C. N. Hinshelwood. *Chemical kinetics of the bacterial cell.* Oxford At The Clarendon Press; London, 1946.

[30] P. Sabatier. Hydrogénations et Deshydrogénations Par Catalyse. *Berichte der deutschen chemischen Gesellschaft* **44**.3 (1911), 1984–2001.

[31] I. Chorkendorff and J. W. Niemantsverdriet. *Concepts of Modern Catalysis and Kinetics.* John Wiley & Sons, 2006.

[32] B. Hammer and J. K. Nørskov. "Theoretical Surface Science and Catalysis—Calculations and Concepts". *Advances in Catalysis.* Vol. 45. Impact of Surface Science on Catalysis. Academic Press, 2000, pp. 71–129. DOI: 10.1016/S0360-0564(02)45013-4.

[33] F. Calle-Vallejo et al. Fast Prediction of Adsorption Properties for Platinum Nanocatalysts with Generalized Coordination Numbers. *Angewandte Chemie International Edition* **53**.32 (2014), 8316–8319. DOI: 10.1002/anie.201402958.

[34] F. Calle-Vallejo et al. Introducing Structural Sensitivity into Adsorption–Energy Scaling Relations by Means of Coordination Numbers. *Nature Chemistry* **7**.5 (2015), 403–410. DOI: `10.1038/nchem.2226`.

[35] F. Calle-Vallejo et al. Finding Optimal Surface Sites on Heterogeneous Catalysts by Counting Nearest Neighbors. *Science* **350**.6257 (2015), 185–189. DOI: `10.1126/science.aab3501`.

[36] M. Jørgensen and H. Grönbeck. Scaling Relations and Kinetic Monte Carlo Simulations To Bridge the Materials Gap in Heterogeneous Catalysis. *ACS Catalysis* **7**.8 (2017), 5054–5061. DOI: `10.1021/acscatal.7b01194`.

[37] J. N. Brønsted. Acid and Basic Catalysis. *Chemical Reviews* **5**.3 (1928), 231–338. DOI: `10.1021/cr60019a001`.

[38] M. G. Evans and M. Polanyi. Inertia and Driving Force of Chemical Reactions. *Transactions of the Faraday Society* **34**.0 (1938), 11–24. DOI: `10.1039/TF9383400011`.

[39] A. F. Cronstedt. Om En Obekant Bärg Art, Som Kallas Zeolites. *Kongl. Svenska Vetenskaps Academiens Handlingar Stockholm* **17** (1756), 120.

[40] S. Cinar and B. Beler-Baykal. Ion Exchange with Natural Zeolites: An Alternative for Water Softening? *Water Science and Technology* **51**.11 (2005), 71–77. DOI: `10.2166/wst.2005.0392`.

[41] A. Primo and H. Garcia. Zeolites as Catalysts in Oil Refining. *Chemical Society Reviews* **43**.22 (2014), 7548–7561. DOI: `10.1039/C3CS60394F`.

[42] I. Yamane and T. Nakazawa. Development of Zeolite for Non-Phosphated Detergents in Japan. *Pure and Applied Chemistry* **58**.10 (1986), 1397–1404. DOI: `10.1351/pac198658101397`.

[43] G. Blanchard, M. Maunaye, and G. Martin. Removal of Heavy Metals from Waters by Means of Natural Zeolites. *Water Research* **18**.12 (1984), 1501–1507. DOI: `10.1016/0043-1354(84)90124-6`.

[44] K. Narsimhan et al. Catalytic Oxidation of Methane into Methanol over Copper-Exchanged Zeolites with Oxygen at Low Temperature. *ACS Central Science* **2**.6 (2016), 424–429. DOI: `10.1021/acscentsci.6b00139`.

[45] B. Ipek and R. F. Lobo. Catalytic Conversion of Methane to Methanol on Cu-SSZ-13 Using N2O as Oxidant. *Chemical Communications* **52**.91 (2016), 13401–13404. DOI: `10.1039/C6CC07893A`.

[46] R. P. Feynman and R. Leighton. *Surely You're Joking, Mr. Feynman!* p. 70. W.W. Norton (USA), 1985.

[47] E. Schrödinger. Quantisierung Als Eigenwertproblem. *Annalen der Physik* **385**.13 (1926), 437–490. DOI: `10.1002/andp.19263851302`.

[48] R. M. Martin. *Electronic Structure: Basic Theory and Practical Methods*. Cambridge: Cambridge Univ. Press, 2004.

[49] J. Thijssen. *Computational Physics*. Cambridge University Press, 2007.

[50] M. Born and R. Oppenheimer. Zur Quantentheorie Der Molekeln. *Annalen der Physik* **389**.20 (1927), 457–484. DOI: `10.1002/andp.19273892002`.

[51] J. Kohanoff. *Electronic Structure Calculations for Solids and Molecules: Theory and Computational Methods*. Cambridge University Press, 2006.

[52] J. C. Slater. The Theory of Complex Spectra. *Physical Review* **34**.10 (1929), 1293–1322. DOI: 10.1103/PhysRev.34.1293.

[53] D. R. Hartree. The Wave Mechanics of an Atom with a Non-Coulomb Central Field. Part I. Theory and Methods. *Mathematical Proceedings of the Cambridge Philosophical Society* **24**.1 (1928), 89–110. DOI: 10.1017/S0305004100011919.

[54] J. C. Slater. The Self Consistent Field and the Structure of Atoms. *Physical Review* **32**.3 (1928), 339–348. DOI: 10.1103/PhysRev.32.339.

[55] J. A. Gaunt. A Theory of Hartree's Atomic Fields. *Mathematical Proceedings of the Cambridge Philosophical Society* **24**.2 (1928), 328–342. DOI: 10.1017/S0305004100015851.

[56] J. C. Slater. Note on Hartree's Method. *Physical Review* **35**.2 (1930), 210–211. DOI: 10.1103/PhysRev.35.210.2.

[57] V. Fock. Näherungsmethode zur Lösung des quantenmechanischen Mehrkörperproblems. *Zeitschrift für Physik* **61**.1 (1930), 126–148. DOI: 10.1007/BF01340294.

[58] D. R. Hartree and W. Hartree. Self-Consistent Field, with Exchange, for Beryllium. *Proceedings of the Royal Society of London. Series A - Mathematical and Physical Sciences* **150**.869 (1935), 9–33. DOI: 10.1098/rspa.1935.0085.

[59] W. Kohn. *Walter Kohn - Nobel Lecture: Electronic Structure of Matter - Wave Functions and Density Functionals*. 1998. URL: https://www.nobelprize.org/prizes/chemistry/1998/kohn/lecture/ (visited on 04/03/2019).

[60] C. Møller and M. S. Plesset. Note on an Approximation Treatment for Many-Electron Systems. *Phys. Rev.* **46**.7 (1934), 618–622. DOI: 10.1103/PhysRev.46.618. URL: https://link.aps.org/doi/10.1103/PhysRev.46.618 (visited on 09/01/2017).

[61] L. H. Thomas. The Calculation of Atomic Fields. *Mathematical Proceedings of the Cambridge Philosophical Society* **23**.05 (1927), 542. DOI: 10.1017/S0305004100011683.

[62] E. Fermi. Statistical Method to Determine Some Properties of Atoms. *Rend. Accad. Naz. Lincei* **6** (1927), 602–607.

[63] P. Hohenberg and W. Kohn. Inhomogeneous Electron Gas. *Physical Review* **136**.3B (1964), B864–B871. DOI: 10.1103/PhysRev.136.B864.

[64] J. J. Sakurai and J. Napolitano. *Modern Quantum Mechanics*. 2. ed. Reading, Mass.: Addison-Wesley, 2011.

[65] W. Kohn and L. J. Sham. Self-Consistent Equations Including Exchange and Correlation Effects. *Physical Review* **140**.4A (1965), A1133–A1138. DOI: 10.1103/PhysRev.140.A1133.

[66] D. Vanderbilt. Soft Self-Consistent Pseudopotentials in a Generalized Eigenvalue Formalism. *Physical Review B* **41**.11 (1990), 7892–7895. DOI: 10.1103/PhysRevB.41.7892.

[67] P. E. Blöchl. Projector Augmented-Wave Method. *Physical Review B* **50**.24 (1994), 17953–17979. DOI: 10.1103/PhysRevB.50.17953.

[68] J. Enkovaara et al. Electronic Structure Calculations with GPAW: A Real-Space Implementation of the Projector Augmented-Wave Method. *Journal of Physics: Condensed Matter* **22**.25 (2010), 253202. DOI: 10.1088/0953-8984/22/25/253202.

[69] G. Kresse and D. Joubert. From Ultrasoft Pseudopotentials to the Projector Augmented-Wave Method. *Physical Review B* **59**.3 (1999), 1758–1775. DOI: `10.1103/PhysRevB.59.1758`.

[70] J. P. Perdew and K. Schmidt. "Jacob's Ladder of Density Functional Approximations for the Exchange-Correlation Energy". Vol. 577. AIP Publishing, 2001, pp. 1–20. DOI: `10.1063/1.1390175`.

[71] A. D. Becke. Perspective: Fifty Years of Density-Functional Theory in Chemical Physics. *The Journal of Chemical Physics* **140**.18 (2014), 18A301. DOI: `10.1063/1.4869598`.

[72] D. M. Ceperley and B. J. Alder. Ground State of the Electron Gas by a Stochastic Method. *Physical Review Letters* **45**.7 (1980), 566–569. DOI: `10.1103/PhysRevLett.45.566`.

[73] O. Gunnarsson, B. I. Lundqvist, and S. Lundqvist. Screening in a Spin-Polarized Electron Liquid. *Solid State Communications* **11**.1 (1972), 149–153. DOI: `10.1016/0038-1098(72)91150-7`.

[74] O. Gunnarsson and B. I. Lundqvist. Exchange and Correlation in Atoms, Molecules, and Solids by the Spin-Density-Functional Formalism. *Physical Review B* **13**.10 (1976), 4274–4298. DOI: `10.1103/PhysRevB.13.4274`.

[75] D. C. Langreth and M. J. Mehl. Beyond the Local-Density Approximation in Calculations of Ground-State Electronic Properties. *Physical Review B* **28**.4 (1983), 1809–1834. DOI: `10.1103/PhysRevB.28.1809`. (Visited on 05/08/2017).

[76] A. D. Becke. Density Functional Calculations of Molecular Bond Energies. *The Journal of Chemical Physics* **84**.8 (1986), 4524–4529. DOI: `10.1063/1.450025`.

[77] J. P. Perdew, K. Burke, and M. Ernzerhof. Generalized Gradient Approximation Made Simple. *Physical Review Letters* **77**.18 (1996), 3865–3868. DOI: `10.1103/PhysRevLett.77.3865`.

[78] S. Kurth, J. P. Perdew, and P. Blaha. Molecular and Solid-State Tests of Density Functional Approximations: LSD, GGAs, and Meta-GGAs. *International Journal of Quantum Chemistry* **75**.4-5 (1999), 889–909.

[79] J. P. Perdew et al. Accurate Density Functional with Correct Formal Properties: A Step Beyond the Generalized Gradient Approximation. *Physical Review Letters* **82**.12 (1999), 2544–2547. DOI: `10.1103/PhysRevLett.82.2544`.

[80] A. D. Becke. A New Mixing of Hartree–Fock and Local Density-functional Theories. *The Journal of Chemical Physics* **98**.2 (1993), 1372–1377. DOI: `10.1063/1.464304`.

[81] D. Bohm and D. Pines. A Collective Description of Electron Interactions: III. Coulomb Interactions in a Degenerate Electron Gas. *Physical Review* **92**.3 (1953), 609–625. DOI: `10.1103/PhysRev.92.609`.

[82] D. C. Langreth and J. P. Perdew. Exchange-Correlation Energy of a Metallic Surface: Wave-Vector Analysis. *Physical Review B* **15**.6 (1977), 2884–2901. DOI: `10.1103/PhysRevB.15.2884`.

[83] X. Ren et al. Random-Phase Approximation and Its Applications in Computational Chemistry and Materials Science. *Journal of Materials Science* **47**.21 (2012), 7447–7471. DOI: `10.1007/s10853-012-6570-4`.

[84] J. Sun, A. Ruzsinszky, and J. P. Perdew. Strongly Constrained and Appropriately Normed Semilocal Density Functional. *Physical Review Letters* **115**.3 (2015), 036402. DOI: `10.1103/PhysRevLett.115.036402`.

[85] S. Grimme. Semiempirical GGA-Type Density Functional Constructed with a Long-Range Dispersion Correction. *Journal of Computational Chemistry* **27**.15 (2006), 1787–1799. DOI: `10.1002/jcc.20495`.

[86] J. E. Jones. On the Determination of Molecular Fields. II. From the Equation of State of a Gas. *Proceedings of the Royal Society of London A: Mathematical, Physical and Engineering Sciences* **106**.738 (1924), 463–477. DOI: `10.1098/rspa.1924.0082`.

[87] J. E. Lennard-Jones. Cohesion. *Proceedings of the Physical Society* **43**.5 (1931), 461. DOI: `10.1088/0959-5309/43/5/301`. (Visited on 04/19/2017).

[88] A. Tkatchenko and M. Scheffler. Accurate Molecular Van Der Waals Interactions from Ground-State Electron Density and Free-Atom Reference Data. *Physical Review Letters* **102**.7 (2009), 073005. DOI: `10.1103/PhysRevLett.102.073005`.

[89] M. Dion et al. Van Der Waals Density Functional for General Geometries. *Physical Review Letters* **92**.24 (2004), 246401. DOI: `10.1103/PhysRevLett.92.246401`.

[90] J. Klimeš, D. R. Bowler, and A. Michaelides. Van Der Waals Density Functionals Applied to Solids. *Physical Review B* **83**.19 (2011), 195131. DOI: `10.1103/PhysRevB.83.195131`.

[91] A. D. Becke. On the Large-gradient Behavior of the Density Functional Exchange Energy. *The Journal of Chemical Physics* **85**.12 (1986), 7184–7187. DOI: `10.1063/1.451353`. (Visited on 04/19/2017).

[92] J. Wellendorff et al. Density Functionals for Surface Science: Exchange-Correlation Model Development with Bayesian Error Estimation. *Physical Review B* **85**.23 (2012), 235149. DOI: `10.1103/PhysRevB.85.235149`.

[93] J. J. Mortensen, L. B. Hansen, and K. W. Jacobsen. Real-Space Grid Implementation of the Projector Augmented Wave Method. *Physical Review B* **71**.3 (2005), 035109. DOI: `10.1103/PhysRevB.71.035109`.

[94] H. Grönbeck. First Principles Studies of Metal-Oxide Surfaces. *Topics in Catalysis* **28**.1-4 (2004), 59–69. DOI: `10.1023/B:TOCA.0000024334.52677.67`.

[95] L. Pauling. *Linus Pauling - Nobel Lecture: Modern Structural Chemistry*. 1954. URL: `https://www.nobelprize.org/prizes/chemistry/1954/pauling/lecture/` (visited on 04/03/2019).

[96] H. Stoll, G. Wagenblast, and H. Preuß. On the Use of Local Basis Sets for Localized Molecular Orbitals. *Theoretica chimica acta* **57**.2 (1980), 169–178. DOI: `10.1007/BF00574903`.

[97] S. Saebo and P. Pulay. Local Treatment of Electron Correlation. *Annual Review of Physical Chemistry* **44**.1 (1993), 213–236. DOI: `10.1146/annurev.pc.44.100193.001241`.

[98] J. Pople. *John Pople - Nobel Lecture: Quantum Chemical Models*. 1998. URL: `https://www.nobelprize.org/prizes/chemistry/1998/pople/lecture/` (visited on 04/03/2019).

[99] P. Pulay. Ab Initio Calculation of Force Constants and Equilibrium Geometries in Polyatomic Molecules. *Molecular Physics* **17**.2 (1969), 197–204. DOI: `10.1080/00268976900100941`.

[100] B. Delley. An All-electron Numerical Method for Solving the Local Density Functional for Polyatomic Molecules. *The Journal of Chemical Physics* **92**.1 (1990), 508–517. DOI: `10.1063/1.458452`.

[101] G. Kresse and J. Furthmüller. Efficiency of Ab-Initio Total Energy Calculations for Metals and Semiconductors Using a Plane-Wave Basis Set. *Computational Materials Science* **6**.1 (1996), 15–50. DOI: `10.1016/0927-0256(96)00008-0`.

[102] G. Kresse and J. Furthmüller. Efficient Iterative Schemes for Ab Initio Total-Energy Calculations Using a Plane-Wave Basis Set. *Physical Review B* **54**.16 (1996), 11169–11186. DOI: `10.1103/PhysRevB.54.11169`.

[103] H. J. Monkhorst and J. D. Pack. Special Points for Brillouin-Zone Integrations. *Physical Review B* **13**.12 (1976), 5188–5192. DOI: `10.1103/PhysRevB.13.5188`.

[104] M. Valter. Personal communication. 2019.

[105] H. S. Taylor. A Theory of the Catalytic Surface. *Proceedings of the Royal Society of London A: Mathematical, Physical and Engineering Sciences* **108**.745 (1925), 105–111. DOI: `10.1098/rspa.1925.0061`.

[106] H. Hellmann. *Einführung in die Quantenchemie*. Leipzig: Franz Deuticke, 1937.

[107] R. P. Feynman. Forces in Molecules. *Physical Review* **56**.4 (1939), 340–343. DOI: `10.1103/PhysRev.56.340`.

[108] J. P. Perdew and S. Kurth. "Density Functionals for Non-Relativistic Coulomb Systems". *Density Functionals: Theory and Applications*. Ed. by D. Joubert. Vol. 500. Springer Berlin Heidelberg, 1998, pp. 8–59. DOI: `10.1007/BFb0106732`.

[109] J. D. Head and M. C. Zerner. A Broyden—Fletcher—Goldfarb—Shanno Optimization Procedure for Molecular Geometries. *Chemical Physics Letters* **122**.3 (1985), 264–270. DOI: `10.1016/0009-2614(85)80574-1`.

[110] B. M. Deb. Note on an Upper Bound Property of Second Derivatives of the Energy. *Chemical Physics Letters* **17**.1 (1972), 78–79. DOI: `10.1016/0009-2614(72)80329-4`.

[111] D. A. McQuarrie and J. D. Simon. Physical Chemistry: A Molecular Approach. *University Science Book* (1997).

[112] D. O. Lindroth. *Thermal Transport in van Der Waals Solids and Inorganic Clathrates from First-Principles Calculations*. Chalmers University of Technology, 2018.

[113] S. Arrhenius. Über Die Reaktionsgeschwindigkeit Bei Der Inversion von Rohrzucker Durch Säuren. *Zeitschrift für Physikalische Chemie* **4**.1 (1889), 226–248. DOI: `10.1515/zpch-1889-0116`.

[114] S. R. Logan. The Origin and Status of the Arrhenius Equation. *Journal of Chemical Education* **59**.4 (1982), 279. DOI: `10.1021/ed059p279`.

[115] G. Henkelman, B. P. Uberuaga, and H. Jónsson. A Climbing Image Nudged Elastic Band Method for Finding Saddle Points and Minimum Energy Paths. *The Journal of Chemical Physics* **113**.22 (2000), 9901–9904. DOI: `10.1063/1.1329672`.

[116] G. Henkelman and H. Jónsson. Improved Tangent Estimate in the Nudged Elastic Band Method for Finding Minimum Energy Paths and Saddle Points. *The Journal of Chemical Physics* **113**.22 (2000), 9978–9985. DOI: 10.1063/1.1323224.

[117] D. Sheppard, R. Terrell, and G. Henkelman. Optimization Methods for Finding Minimum Energy Paths. *The Journal of Chemical Physics* **128**.13 (2008), 134106. DOI: 10.1063/1.2841941.

[118] G. Henkelman and H. Jónsson. A Dimer Method for Finding Saddle Points on High Dimensional Potential Surfaces Using Only First Derivatives. *The Journal of Chemical Physics* **111**.15 (1999), 7010–7022. DOI: 10.1063/1.480097.

[119] A. Heyden, A. T. Bell, and F. J. Keil. Efficient Methods for Finding Transition States in Chemical Reactions: Comparison of Improved Dimer Method and Partitioned Rational Function Optimization Method. *The Journal of Chemical Physics* **123**.22 (2005), 224101. DOI: 10.1063/1.2104507.

[120] T. A. Halgren and W. N. Lipscomb. The Synchronous-Transit Method for Determining Reaction Pathways and Locating Molecular Transition States. *Chemical Physics Letters* **49**.2 (1977), 225–232. DOI: 10.1016/0009-2614(77)80574-5.

[121] P. N. Plessow. Efficient Transition State Optimization of Periodic Structures through Automated Relaxed Potential Energy Surface Scans. *Journal of Chemical Theory and Computation* (2018). DOI: 10.1021/acs.jctc.7b01070.

[122] D. V. Schroeder. *An Introduction to Thermal Physics*. International Edition. San Francisco: Addison Wesley Longman, 2000.

[123] K. Reuter and M. Scheffler. Composition, structure, and stability of $RuO_2(110)$ as a function of oxygen pressure. *Phys. Rev. B* **65**.3 (2001). DOI: 10.1103/PhysRevB.65.035406. URL: https://link.aps.org/doi/10.1103/PhysRevB.65.035406.

[124] D. A. McQuarrie and J. D. Simon. *Molecular thermodynamics*. University Science Books Sausalito, CA, 1999.

[125] T. L. Hill. *An Introduction to Statistical Thermodynamics*. New York: Dover Publications Inc., 1960.

[126] M. Jørgensen and H. Grönbeck. Adsorbate Entropies with Complete Potential Energy Sampling in Microkinetic Modeling. *The Journal of Physical Chemistry C* (2017). DOI: 10.1021/acs.jpcc.6b11487.

[127] A. P. J. Jansen. *An Introduction to Kinetic Monte Carlo Simulations of Surface Reactions*. Springer-Verlag Berlin Heidelberg, 2012.

[128] H. Eyring. The Activated Complex in Chemical Reactions. *The Journal of Chemical Physics* **3**.2 (1935), 107–115. DOI: 10.1063/1.1749604.

[129] M. G. Evans and M. Polanyi. Some Applications of the Transition State Method to the Calculation of Reaction Velocities, Especially in Solution. *Transactions of the Faraday Society* **31** (1935), 875–894.

[130] G. Mills, H. Jónsson, and G. K. Schenter. Reversible Work Transition State Theory: Application to Dissociative Adsorption of Hydrogen. *Surface Science* **324**.2–3 (1995), 305–337. DOI: 10.1016/0039-6028(94)00731-4.

[131] C. T. Campbell. Future Directions and Industrial Perspectives Micro- and Macro-Kinetics: Their Relationship in Heterogeneous Catalysis. *Topics in Catalysis* **1**.3-4 (1994), 353–366. DOI: 10.1007/BF01492288.

[132] C. Stegelmann, A. Andreasen, and C. T. Campbell. Degree of Rate Control: How Much the Energies of Intermediates and Transition States Control Rates. *Journal of the American Chemical Society* **131**.23 (2009), 8077–8082. DOI: 10.1021/ja9000097.

[133] I. Langmuir. The Evaporation, Condensation and Reflection of Molecules and the Mechanism of Adsorption. *Physical Review* **8**.2 (1916), 149–176. DOI: 10.1103/PhysRev.8.149.

[134] P. A. Redhead. Thermal Desorption of Gases. *Vacuum* **12**.4 (1962), 203–211. DOI: 10.1016/0042-207X(62)90978-8.

[135] M. Niwa et al. Temperature-Programmed Desorption of Ammonia with Readsorption Based on the Derived Theoretical Equation. *The Journal of Physical Chemistry* **99**.21 (1995), 8812–8816. DOI: 10.1021/j100021a056.

[136] L. Chen et al. Interpretation of NH3-TPD Profiles from Cu-CHA Using First-Principles Calculations. *Topics in Catalysis* (2018). DOI: 10.1007/s11244-018-1095-y.

[137] P. Tang et al. Methane Activation: The Past and Future. *Energy & Environmental Science* **7**.8 (2014), 2580–2591. DOI: 10.1039/C4EE00604F.

[138] R. Horn and R. Schlögl. Methane Activation by Heterogeneous Catalysis. *Catalysis Letters* **145**.1 (2015), 23–39. DOI: 10.1007/s10562-014-1417-z.

[139] A. P. E. York, T. Xiao, and M. L. H. Green. Brief Overview of the Partial Oxidation of Methane to Synthesis Gas. *Topics in Catalysis* **22**.3-4 (2003), 345–358. DOI: 10.1023/A:1023552709642.

[140] A. Holmen. Direct Conversion of Methane to Fuels and Chemicals. *Catalysis Today* **142**.1–2 (2009), 2–8. DOI: 10.1016/j.cattod.2009.01.004.

[141] P. Tomkins, M. Ranocchiari, and J. A. van Bokhoven. Direct Conversion of Methane to Methanol under Mild Conditions over Cu-Zeolites and Beyond. *Accounts of Chemical Research* **50**.2 (2017), 418–425. DOI: 10.1021/acs.accounts.6b00534.

[142] I. Dybkjær and K. Aasberg-Petersen. Synthesis Gas Technology Large-Scale Applications. *The Canadian Journal of Chemical Engineering* **94**.4 (2016), 607–612. DOI: 10.1002/cjce.22453.

[143] K. Tabata et al. Activation of Methane by Oxygen and Nitrogen Oxides. *Catalysis Reviews* **44**.1 (2002), 1–58. DOI: 10.1081/CR-120001458.

[144] M.-L. Tsai et al. [Cu2O]2+ Active Site Formation in Cu–ZSM-5: Geometric and Electronic Structure Requirements for N2O Activation. *Journal of the American Chemical Society* **136**.9 (2014), 3522–3529. DOI: 10.1021/ja4113808.

[145] V. L. Sushkevich et al. Selective Anaerobic Oxidation of Methane Enables Direct Synthesis of Methanol. *Science* **356**.6337 (2017), 523–527. DOI: 10.1126/science.aam9035.

[146] J. Nilsson. *Operando X-Ray Absorption Spectroscopy Studies of Methane Oxidation Catalysts*. Chalmers University of Technology, 2017.

[147] A. Trinchero, A. Hellman, and H. Grönbeck. Methane Oxidation over Pd and Pt Studied by DFT and Kinetic Modeling. *Surface Science* **616** (2013), 206–213. DOI: 10.1016/j.susc.2013.06.014.

[148] M. V. den Bossche and H. Grönbeck. Methane Oxidation over PdO(101) Revealed by First-Principles Kinetic Modeling. *Journal of the American Chemical Society* **137**.37 (2015), 12035–12044. DOI: 10.1021/jacs.5b06069.

[149] M. Jørgensen and H. Grönbeck. First-Principles Microkinetic Modeling of Methane Oxidation over Pd(100) and Pd(111). *ACS Catalysis* (2016), 6730–6738. DOI: 10.1021/acscatal.6b01752.

[150] B. E. R. Snyder et al. Iron and Copper Active Sites in Zeolites and Their Correlation to Metalloenzymes. *Chemical Reviews* **118**.5 (2018), 2718–2768. DOI: 10.1021/acs.chemrev.7b00344.

[151] J. M. Thomas, R. Raja, and D. W. Lewis. Single-Site Heterogeneous Catalysts. *Angewandte Chemie International Edition* **44**.40 (2005), 6456–6482. DOI: 10.1002/anie.200462473.

[152] A. C. Rosenzweig et al. Crystal Structure of a Bacterial Non-Haem Iron Hydroxylase That Catalyses the Biological Oxidation of Methane. *Nature* **366**.6455 (1993), 537–543. DOI: 10.1038/366537a0.

[153] R. Balasubramanian et al. Oxidation of Methane by a Biological Dicopper Centre. *Nature* **465**.7294 (2010), 115–119. DOI: 10.1038/nature08992.

[154] A. E. Shilov and A. A. Shteinman. Methane Hydroxylation: A Biomimetic Approach. *Russian Chemical Reviews* **81**.4 (2012), 291. DOI: 10.1070/RC2012v081n04ABEH004271.

[155] M. H. Mahyuddin et al. Theoretical Overview of Methane Hydroxylation by Copper–Oxygen Species in Enzymatic and Zeolitic Catalysts. *Accounts of Chemical Research* **51**.10 (2018), 2382–2390. DOI: 10.1021/acs.accounts.8b00236.

[156] D. H. Olson et al. Crystal Structure and Structure-Related Properties of ZSM-5. *The Journal of Physical Chemistry* **85**.15 (1981), 2238–2243. DOI: 10.1021/j150615a020.

[157] M. Beller, A. Renken, and R. A. van Santen. *Catalysis*. Wiley-VCH, Weinheim, 2012.

[158] M. H. Groothaert et al. Selective Oxidation of Methane by the Bis(μ-Oxo)Dicopper Core Stabilized on ZSM-5 and Mordenite Zeolites. *Journal of the American Chemical Society* **127**.5 (2005), 1394–1395. DOI: 10.1021/ja047158u.

[159] J. Shan et al. Conversion of Methane to Methanol with a Bent Mono(μ-Oxo)Dinickel Anchored on the Internal Surfaces of Micropores. *Langmuir* **30**.28 (2014), 8558–8569. DOI: 10.1021/la501184b.

[160] N. V. Beznis, B. M. Weckhuysen, and J. H. Bitter. Partial Oxidation of Methane Over Co-ZSM-5: Tuning the Oxygenate Selectivity by Altering the Preparation Route. *Catalysis Letters* **136**.1-2 (2010), 52–56. DOI: 10.1007/s10562-009-0206-6.

[161] E. V. Starokon et al. Room-Temperature Oxidation of Methane by α-Oxygen and Extraction of Products from the FeZSM-5 Surface. *The Journal of Physical Chemistry C* **115**.5 (2011), 2155–2161. DOI: 10.1021/jp109906j.

[162] S. E. Bozbag et al. Methane to Methanol over Copper Mordenite: Yield Improvement through Multiple Cycles and Different Synthesis Techniques. *Catalysis Science & Technology* **6**.13 (2016), 5011–5022. DOI: 10.1039/C6CY00041J.

[163] M. J. Wulfers et al. Conversion of Methane to Methanol on Copper-Containing Small-Pore Zeolites and Zeotypes. *Chemical Communications* **51**.21 (2015), 4447–4450. DOI: 10.1039/C4CC09645B.

[164] A. R. Kulkarni et al. Cation-Exchanged Zeolites for the Selective Oxidation of Methane to Methanol. *Catalysis Science & Technology* (2017). DOI: 10.1039/C7CY01229B.

[165] J. J. Pluth, J. V. Smith, and W. J. Mortier. Positions of Cations and Molecules in Zeolites with the Chabazite Framework. IV Hydrated and Dehydrated Cu2+-Exchanged Chabazite. *Materials Research Bulletin* **12**.10 (1977), 1001–1007. DOI: 10.1016/0025-5408(77)90025-3.

[166] N. V. Beznis, B. M. Weckhuysen, and J. H. Bitter. Cu-ZSM-5 Zeolites for the Formation of Methanol from Methane and Oxygen: Probing the Active Sites and Spectator Species. *Catalysis Letters* **138**.1-2 (2010), 14–22. DOI: 10.1007/s10562-010-0380-6.

[167] B. R. Goodman et al. Statistical Analysis of Al Distributions and Metal Ion Pairing Probabilities in Zeolites. *Catalysis Letters* **68**.1-2 (2000), 85–93. DOI: 10.1023/A:1019066916541.

[168] W. Loewenstein. The Distribution of Aluminum in the Tetrahedra of Silicates and Aluminates. *American Mineralogist* **39**.1-2 (1954), 92–96.

[169] R. G. Bell, R. A. Jackson, and C. R. A. Catlow. Löwenstein's Rule in Zeolite A: A Computational Study. *Zeolites* **12**.7 (1992), 870–871.

[170] O. H. Han, C.-S. Kim, and S. B. Hong. Direct Evidence for the Nonrandom Nature of Al Substitution in Zeolite ZSM-5: An Investigation by 27Al MAS and MQ MAS NMR. *Angewandte Chemie* **114**.3 (2002), 487–490. DOI: 10.1002/1521-3757(20020201)114:3<487::AID-ANGE487>3.0.CO;2-Z.

[171] V. Gábová, J. Dědeček, and J. Čejka. Control of Al Distribution in ZSM-5 by Conditions of Zeolite Synthesis. *Chemical Communications* 10 (2003), 1196–1197. DOI: 10.1039/B301634J.

[172] G. J. Kramer et al. Understanding the Acid Behaviour of Zeolites from Theory and Experiment. *Nature* **363**.6429 (1993), 529. DOI: 10.1038/363529a0.

[173] W. Vermeiren and J.-P. Gilson. Impact of Zeolites on the Petroleum and Petrochemical Industry. *Topics in Catalysis* **52**.9 (2009), 1131–1161. DOI: 10.1007/s11244-009-9271-8.

[174] C. Martínez and A. Corma. Inorganic Molecular Sieves: Preparation, Modification and Industrial Application in Catalytic Processes. *Coordination Chemistry Reviews*. Industrial Chemistry **255**.13 (2011), 1558–1580. DOI: 10.1016/j.ccr.2011.03.014.

[175] M. Wang et al. Genesis and Stability of Hydronium Ions in Zeolite Channels. *Journal of the American Chemical Society* (2019). DOI: 10.1021/jacs.8b07969.

[176] G. Li et al. Stability and Reactivity of Copper Oxo-Clusters in ZSM-5 Zeolite for Selective Methane Oxidation to Methanol. *Journal of Catalysis* **338** (2016), 305–312. DOI: 10.1016/j.jcat.2016.03.014.

[177] P. J. Smeets, M. H. Groothaert, and R. A. Schoonheydt. Cu Based Zeolites: A UV–vis Study of the Active Site in the Selective Methane Oxidation at Low

Temperatures. *Catalysis Today* **110**.3–4 (2005), 303–309. DOI: 10.1016/j.cattod.2005.09.028.

[178] P. J. Smeets et al. Oxygen Precursor to the Reactive Intermediate in Methanol Synthesis by Cu-ZSM-5. *Journal of the American Chemical Society* **132**.42 (2010), 14736–14738. DOI: 10.1021/ja106283u.

[179] P. Tomkins et al. Isothermal Cyclic Conversion of Methane into Methanol over Copper-Exchanged Zeolite at Low Temperature. *Angewandte Chemie* **128**.18 (2016), 5557–5561. DOI: 10.1002/ange.201511065.

[180] P. Vanelderen et al. Cu-ZSM-5: A Biomimetic Inorganic Model for Methane Oxidation. *Journal of Catalysis*. Molecular Approach to Heterogeneous Catalysis. **284**.2 (2011), 157–164. DOI: 10.1016/j.jcat.2011.10.009.

[181] J. S. Woertink et al. A [Cu2O]2+ Core in Cu-ZSM-5, the Active Site in the Oxidation of Methane to Methanol. *Proceedings of the National Academy of Sciences* **106**.45 (2009), 18908–18913. DOI: 10.1073/pnas.0910461106.

[182] M. H. Mahyuddin et al. Direct Conversion of Methane to Methanol by Metal-Exchanged ZSM-5 Zeolite (Metal = Fe, Co, Ni, Cu). *ACS Catalysis* (2016), 8321–8331. DOI: 10.1021/acscatal.6b01721.

[183] T. Yumura et al. Roles of Water Molecules in Modulating the Reactivity of Dioxygen-Bound Cu-ZSM-5 toward Methane: A Theoretical Prediction. *ACS Catalysis* (2016), 2487–2495. DOI: 10.1021/acscatal.5b02477.

[184] P. Haack et al. Access to a CuII–O–CuII Motif: Spectroscopic Properties, Solution Structure, and Reactivity. *Journal of the American Chemical Society* **135**.43 (2013), 16148–16160. DOI: 10.1021/ja406721a.

[185] Z.-J. Zhao et al. Theoretical Insights into the Selective Oxidation of Methane to Methanol in Copper-Exchanged Mordenite. *ACS Catalysis* (2016), 3760–3766. DOI: 10.1021/acscatal.6b00440.

[186] E. Borfecchia et al. Evolution of Active Sites during Selective Oxidation of Methane to Methanol over Cu-CHA and Cu-MOR Zeolites as Monitored by Operando XAS. *Catalysis Today* (2018). DOI: 10.1016/j.cattod.2018.07.028.

[187] M. H. Groothaert et al. Identification of Cu(II) Coordination Structures in Cu-ZSM-5, Based on a DFT/Ab Initio Assignment of the EPR Spectra. *Physical Chemistry Chemical Physics* **5**.10 (2003), 2135–2144. DOI: 10.1039/B301120H.

[188] B. F. Mentzen and G. Bergeret. Crystallographic Determination of the Positions of the Copper Cations in Zeolite MFI. *The Journal of Physical Chemistry C* **111**.34 (2007), 12512–12516. DOI: 10.1021/jp075452d.

[189] T. Yumura et al. Effects of ZSM-5 Zeolite Confinement on Reaction Intermediates during Dioxygen Activation by Enclosed Dicopper Cations. *Inorganic Chemistry* **48**.2 (2009), 508–517. DOI: 10.1021/ic8010184.

[190] N. V. Beznis et al. Oxidation of Methane to Methanol and Formaldehyde over Co–ZSM-5 Molecular Sieves: Tuning the Reactivity and Selectivity by Alkaline and Acid Treatments of the Zeolite ZSM-5 Agglomerates. *Microporous and Mesoporous Materials* **138**.1–3 (2011), 176–183. DOI: 10.1016/j.micromeso.2010.09.009.

[191] E. V. Starokon et al. Mechanisms of Iron Activation on Fe-Containing Zeolites and the Charge of α-Oxygen. *Topics in Catalysis* **23**.1-4 (2003), 137–143. DOI: 10.1023/A:1024832606400.

[192] C. Hammond et al. Direct Catalytic Conversion of Methane to Methanol in an Aqueous Medium by Using Copper-Promoted Fe-ZSM-5. *Angewandte Chemie International Edition* **51**.21 (2012), 5129–5133. DOI: 10.1002/anie.201108706.

[193] D. Nachtigallová et al. Coordination and Siting of Cu+ Ions in ZSM-5: A Combined Quantum Mechanics/Interatomic Potential Function Study. *Physical Chemistry Chemical Physics* **1**.8 (1999), 2019–2026. DOI: 10.1039/A900214F.

[194] A. B. Ene et al. Adsorption of Oxygen on Copper in Cu/HZSM5 Zeolites. *Physical Chemistry Chemical Physics* **12**.24 (2010), 6520–6531. DOI: 10.1039/C000750A.

[195] G. Li et al. Stability of Extraframework Iron-Containing Complexes in ZSM-5 Zeolite. *The Journal of Physical Chemistry C* **117**.1 (2013), 413–426. DOI: 10.1021/jp310374k.

[196] P. Vanelderen et al. Spectroscopic Definition of the Copper Active Sites in Mordenite: Selective Methane Oxidation. *Journal of the American Chemical Society* **137**.19 (2015), 6383–6392. DOI: 10.1021/jacs.5b02817.

[197] E. M. C. Alayon et al. Reaction Conditions of Methane-to-Methanol Conversion Affect the Structure of Active Copper Sites. *ACS Catalysis* **4**.1 (2014), 16–22. DOI: 10.1021/cs400713c.

[198] E. M. C. Alayon et al. Bis(μ-Oxo) versus Mono(μ-Oxo)Dicopper Cores in a Zeolite for Converting Methane to Methanol: An in Situ XAS and DFT Investigation. *Physical Chemistry Chemical Physics* **17**.12 (2015), 7681–7693. DOI: 10.1039/C4CP03226H.

[199] F. Göltl et al. Computationally Exploring Confinement Effects in the Methane-to-Methanol Conversion Over Iron-Oxo Centers in Zeolites. *ACS Catalysis* (2016), 8404–8409. DOI: 10.1021/acscatal.6b02640.

[200] M. He et al. Theoretical Study on Methane Oxidation Catalyzed by Fe/ZSM-5: The Significant Role of Water on Binuclear Iron Active Sites. *The Journal of Physical Chemistry C* (2016). DOI: 10.1021/acs.jpcc.6b09548.

[201] C. Paolucci et al. Catalysis in a Cage: Condition-Dependent Speciation and Dynamics of Exchanged Cu Cations in SSZ-13 Zeolites. *Journal of the American Chemical Society* **138**.18 (2016), 6028–6048. DOI: 10.1021/jacs.6b02651.

[202] L. Vilella and F. Studt. The Stability of Copper Oxo Species in Zeolite Frameworks. *European Journal of Inorganic Chemistry* **2016**.10 (2016), 1514–1520. DOI: 10.1002/ejic.201501270.

[203] G. T. Palomino et al. Oxidation States of Copper Ions in ZSM-5 Zeolites. A Multitechnique Investigation. *The Journal of Physical Chemistry B* **104**.17 (2000), 4064–4073. DOI: 10.1021/jp993893u.

[204] F. Göltl, P. Sautet, and I. Hermans. The Impact of Finite Temperature on the Coordination of Cu Cations in the Zeolite SSZ-13. *Catalysis Today*. Advances in Automobile Emissions Control Catalysis **267** (2016), 41–46. DOI: 10.1016/j.cattod.2015.10.028.

[205] S. Grundner et al. Single-Site Trinuclear Copper Oxygen Clusters in Mordenite for Selective Conversion of Methane to Methanol. *Nature Communications* **6** (2015), 7546. DOI: 10.1038/ncomms8546.

[206] A. R. Kulkarni et al. Monocopper Active Site for Partial Methane Oxidation in Cu-Exchanged 8MR Zeolites. *ACS Catalysis* (2016), 6531–6536. DOI: 10.1021/acscatal.6b01895.

[207] D. Palagin et al. Assessing the Relative Stability of Copper Oxide Clusters as Active Sites of a CuMOR Zeolite for Methane to Methanol Conversion: Size Matters? *Nanoscale* **9**.3 (2017), 1144–1153. DOI: 10.1039/C6NR07723D.

[208] A. A. Verma et al. NO Oxidation: A Probe Reaction on Cu-SSZ-13. *Journal of Catalysis* **312** (2014), 179–190. DOI: 10.1016/j.jcat.2014.01.017.

[209] L. Chen et al. Activation of Oxygen on (NH3CuNH3)+ in NH3-SCR over Cu-CHA. *Journal of Catalysis* **358** (2018), 179–186. DOI: 10.1016/j.jcat.2017.12.009.

[210] S. Shwan et al. Solid-State Ion-Exchange of Copper into Zeolites Facilitated by Ammonia at Low Temperature. *ACS Catalysis* **5**.1 (2015), 16–19. DOI: 10.1021/cs5015139.

[211] F. Gao et al. Understanding Ammonia Selective Catalytic Reduction Kinetics over Cu/SSZ-13 from Motion of the Cu Ions. *Journal of Catalysis* **319** (2014), 1–14. DOI: 10.1016/j.jcat.2014.08.010.

[212] A. A. Latimer et al. Understanding Trends in C-H Bond Activation in Heterogeneous Catalysis. *Nature Materials* **16**.2 (2017), 225–229. DOI: 10.1038/nmat4760.

[213] A. A. Latimer et al. Mechanistic Insights into Heterogeneous Methane Activation. *Physical Chemistry Chemical Physics* **19**.5 (2017), 3575–3581. DOI: 10.1039/C6CP08003K.

[214] *Big-Bang Model — Cosmology.* https://global.britannica.com/topic/big-bang-model. (Visited on 04/29/2017).

[215] C. L. Bennett et al. Nine-Year Wilkinson Microwave Anisotropy Probe (WMAP) Observations: Final Maps and Results. *The Astrophysical Journal Supplement Series* **208**.2 (2013), 20. DOI: 10.1088/0067-0049/208/2/20. arXiv: 1212.5225.

[216] Y. Hirata et al. Characterieation of ZSM-5 Zeolite Synthesized from Silica Stone (Ioh Island, Kagoshima Prefecture). *Nippon seramikkusu kyokai gakujutsu ronbunshi* **99**.12 (1991), 1255–1259.

[217] F. Göltl et al. Van Der Waals Interactions between Hydrocarbon Molecules and Zeolites: Periodic Calculations at Different Levels of Theory, from Density Functional Theory to the Random Phase Approximation and Møller-Plesset Perturbation Theory. *The Journal of Chemical Physics* **137**.11 (2012), 114111. DOI: 10.1063/1.4750979.

[218] B. R. Wood et al. Methanol Formation on Fe/Al-MFI via the Oxidation of Methane by Nitrous Oxide. *Journal of Catalysis* **225**.2 (2004), 300–306. DOI: 10.1016/j.jcat.2004.04.010.

[219] S. M. Campbell, X.-Z. Jiang, and R. F. Howe. Methanol to Hydrocarbons: Spectroscopic Studies and the Significance of Extra-Framework Aluminium. *Microporous and Mesoporous Materials* **29** (1999), 91–108.

[220] F. Haase and J. Sauer. Interaction of Methanol with Brønsted Acid Sites of Zeolite Catalysts: An Ab Initio Study. *Journal of the American Chemical Society* **117** (1995), 3780–3789.

[221] P. G. Moses and J. K. Nørskov. Methanol to Dimethyl Ether over ZSM-22: A Periodic Density Functional Theory Study. *ACS Catalysis* **3**.4 (2013), 735–745. DOI: 10.1021/cs300722w.

[222] A. Ghorbanpour, J. D. Rimer, and L. C. Grabow. Computational Assessment of the Dominant Factors Governing the Mechanism of Methanol Dehydration over H-ZSM-5 with Heterogeneous Aluminum Distribution. *ACS Catalysis* **6**.4 (2016), 2287–2298. DOI: 10.1021/acscatal.5b02367.

[223] S. Svelle et al. Mechanistic Aspects of the Zeolite Catalyzed Methylation of Alkenes and Aromatics with Methanol: A Review. *Topics in Catalysis* **54**.13 (2011), 897. DOI: 10.1007/s11244-011-9697-7.

[224] P. N. Plessow and F. Studt. Unraveling the Mechanism of the Initiation Reaction of the Methanol to Olefins Process Using Ab Initio and DFT Calculations. *ACS Catalysis* **7**.11 (2017), 7987–7994. DOI: 10.1021/acscatal.7b03114.

[225] C. Ortega et al. Methanol to Dimethyl Ether Conversion over a ZSM-5 Catalyst: Intrinsic Kinetic Study on an External Recycle Reactor. *Chemical Engineering Journal* **347** (2018), 741–753. DOI: 10.1016/j.cej.2018.04.160.

[226] M. Boronat and A. Corma. What Is Measured When Measuring Acidity in Zeolites with Probe Molecules? *ACS Catalysis* (2019), 1539–1548. DOI: 10.1021/acscatal.8b04317.

[227] M. Reina et al. Conversion of Methyl Mercaptan to Hydrocarbons over H-ZSM-5 Zeolite: DFT/BOMD Study. *ACS Omega* **2**.8 (2017), 4647–4656. DOI: 10.1021/acsomega.7b00756.

[228] M. Jørgensen, L. Chen, and H. Grönbeck. Monte Carlo Potential Energy Sampling for Molecular Entropy in Zeolites. *The Journal of Physical Chemistry C* **122**.35 (2018), 20351–20357. DOI: 10.1021/acs.jpcc.8b05382.

[229] P. J. Dauenhauer and O. A. Abdelrahman. A Universal Descriptor for the Entropy of Adsorbed Molecules in Confined Spaces. *ACS Central Science* **4**.9 (2018), 1235–1243. DOI: 10.1021/acscentsci.8b00419.

[230] S. Creci et al. Tuned Acidity for Catalytic Reactions: Synthesis and Characterization of Fe- and Al-MFI Zeotypes. *Topics in Catalysis* (2019). DOI: 10.1007/s11244-019-01155-4.

[231] A. H. Maslow. The Psychology of Science a Reconnaissance (1966).

[232] J. Sauer and M. Sierka. Combining Quantum Mechanics and Interatomic Potential Functions in Ab Initio Studies of Extended Systems. *Journal of Computational Chemistry* **21**.16 (2000), 1470–1493. DOI: 10.1002/1096-987X(200012)21:16<1470::AID-JCC5>3.0.CO;2-L.

[233] T. Vreven et al. Combining Quantum Mechanics Methods with Molecular Mechanics Methods in ONIOM. *Journal of Chemical Theory and Computation* **2**.3 (2006), 815–826. DOI: 10.1021/ct050289g.

[234] S. Dinda et al. Modeling Catalytic Steps on Extra-Framework Metal Centers in Zeolites. A Case Study on Ethylene Dimerization. *The Journal of Physical Chemistry C* (2014). DOI: 10.1021/jp508141q.

[235] L. Leukkunen, T. Verho, and O. Lopez-Acevedo. A Multi-Scale Code for Flexible Hybrid Simulations. *Computing in Science & Engineering* **16**.2 (2014), 54–62. DOI: 10.1109/MCSE.2013.51. arXiv: 1211.2075.

[236] G. Piccini, M. Alessio, and J. Sauer. Ab Initio Study of Methanol and Ethanol Adsorption on Brønsted Sites in Zeolite H-MFI. *Physical Chemistry Chemical Physics* **20**.30 (2018), 19964–19970. DOI: 10.1039/C8CP03632B.

[237] F. Libisch, C. Huang, and E. A. Carter. Embedded Correlated Wavefunction Schemes: Theory and Applications. *Accounts of Chemical Research* **47**.9 (2014), 2768–2775. DOI: 10.1021/ar500086h.